NAVAL POSTGRADUATE SCHOOL

MONTEREY, CALIFORNIA

THESIS

THE EFFECT OF APPLIED TENSILE STRESS ON LOCALIZED CORROSION IN SENSITIZED AA5083

by

Roy T. Johnston

September 2015

Thesis Advisor:	Sarath K. Menon
Co-Advisor:	Luke N. Brewer

Approved for public release; distribution is unlimited

REPORT DOCUMENTATION PAGE	*Form Approved OMB No. 0704–0188*

1. AGENCY USE ONLY ***(Leave blank)***	**2. REPORT DATE** September 2015	**3. REPORT TYPE AND DATES COVERED** Master’s thesis

4. TITLE AND SUBTITLE THE EFFECT OF APPLIED TENSILE STRESS ON LOCALIZED CORROSION IN SENSITIZED AA5083	**5. FUNDING NUMBERS**
6. AUTHOR(S) Johnston, Roy T.	
7. PERFORMING ORGANIZATION NAME(S) AND ADDRESS(ES) Naval Postgraduate School Monterey, CA 93943-5000	**8. PERFORMING ORGANIZATION REPORT NUMBER**
9. SPONSORING /MONITORING AGENCY NAME(S) AND ADDRESS(ES) N/A	**10. SPONSORING/MONITORING AGENCY REPORT NUMBER**

11. SUPPLEMENTARY NOTES The views expressed in this thesis are those of the author and do not reflect the official policy or position of the Department of Defense or the U.S. government. IRB Protocol number ____N/A____.

12a. DISTRIBUTION / AVAILABILITY STATEMENT Approved for public release;distribution is unlimited	**12b. DISTRIBUTION CODE**

13. ABSTRACT (maximum 200 words)

This thesis describes significant changes in the type and degree of localized corrosion for sensitized AA5083 under an applied tensile stress. AA5083 is an aluminum-magnesium alloy that experiences severe intergranular corrosion and intergranular stress corrosion cracking if sensitized. In this research, AA5083-H116 plates were cut into bend-bar samples along both the rolling and transverse directions, and then sensitized to two different levels using laboratory heat treatments of 7 and 30 days at 100°C. The sensitized samples were subjected to elastic tensile loading using a 4-point bend rig while being exposed to a 0.6 molar saltwater solution. Electrochemical polarization was performed on the tensile regions of the samples while under applied stress. Potentiodynamic scans showed that although sensitization causes the most change in electrochemistry, stress does shift the Tafel plot to be more stable when comparing the values for open circuit potential, but reduces the pitting potential of the passivating oxides. Confocal microscopy showed that samples with applied tensile stress produced a much higher density of localized corrosion, including pitting and intergranular corrosion than samples without applied tensile stress. The degree of corrosion damage was slightly higher for samples loaded in the transverse direction compared to samples loaded in the longitudinal direction.

14. SUBJECT TERMS Aluminum alloy, AA5083, IGSCC, intergranular stress corrosion cracking, localized corrosion, sensitized aluminum	**15. NUMBER OF PAGES** 75
	16. PRICE CODE

17. SECURITY CLASSIFICATION OF REPORT Unclassified	**18. SECURITY CLASSIFICATION OF THIS PAGE** Unclassified	**19. SECURITY CLASSIFICATION OF ABSTRACT** Unclassified	**20. LIMITATION OF ABSTRACT** UU

NSN 7540-01-280-5500

Standard Form 298 (Rev. 2-89)
Prescribed by ANSI Std. 239-18

THIS PAGE INTENTIONALLY LEFT BLANK

THE EFFECT OF APPLIED TENSILE STRESS ON LOCALIZED CORROSION IN SENSITIZED AA5083

Roy T. Johnston
Lieutenant, United States Navy
B.S., The Citadel, 2006

Submitted in partial fulfillment of the
requirements for the degree of

MASTER OF SCIENCE IN MECHANICAL ENGINEERING

from the

NAVAL POSTGRADUATE SCHOOL
June 2015

Author: Roy T. Johnston

Approved by: Sarath K. Menon
Thesis Advisor

Luke N. Brewer
Co-Advisor

Garth V. Hobson
Chair, Department of Mechanical and Aerospace Engineering

THIS PAGE INTENTIONALLY LEFT BLANK

ABSTRACT

This thesis describes significant changes in the type and degree of localized corrosion for sensitized AA5083 under an applied tensile stress. AA5083 is an aluminum-magnesium alloy that experiences severe intergranular corrosion and intergranular stress corrosion cracking if sensitized. In this research, AA5083-H116 plates were cut into bend-bar samples along both the rolling and transverse directions, and then sensitized to two different levels using laboratory heat treatments of 7 and 30 days at 100°C. The sensitized samples were subjected to elastic tensile loading using a 4-point bend rig while being exposed to a 0.6 molar saltwater solution. Electrochemical polarization was performed on the tensile regions of the samples while under applied stress. Potentiodynamic scans showed that although sensitization causes the most change in electrochemistry, stress does shift the Tafel plot to be more stable when comparing the values for open circuit potential, but reduces the pitting potential of the passivating oxides. Confocal microscopy showed that samples with applied tensile stress produced a much higher density of localized corrosion, including pitting and intergranular corrosion than samples without applied tensile stress. The degree of corrosion damage was slightly higher for samples loaded in the transverse direction compared to samples loaded in the longitudinal direction.

THIS PAGE INTENTIONALLY LEFT BLANK

TABLE OF CONTENTS

THIS PAGE INTENTIONALLY LEFT BLANK

LIST OF FIGURES

LIST OF TABLES

LIST OF ACRONYMS AND ABBREVIATIONS

AA5083	Aluminum 5083-H116
DoS	Degree of Sensitization
E_{pit}	Pitting Potential
IGC	Intergranular Corrosion
IGSCC	Intergranular Stress Corrosion Cracking
LCS	Littoral Combat Ship
NAMLT	Nitric Acid Mass Loss Test
OCP	Open Circuit Potential
SCC	Stress Corrosion Cracking
TGSCC	Transgranular Stress Corrosion Cracking

THIS PAGE INTENTIONALLY LEFT BLANK

ACKNOWLEDGMENTS

I want to express my deepest appreciation to Professor Luke Brewer, whose enthusiastic pursuit of knowledge and scientific advancement has motivated me to complete this thesis and continue to grow in all aspects of my life. My appreciation for his patience, compassion, and understanding goes beyond words. I wish you continued success in your future endeavors.

I want to acknowledge other staff members at Naval Postgraduate School. I would like to thank Professor Dragoslav Grbovic for his guidance and for allowing me to use his facilities to perform my measurements, and Alex Fuhrmann for his tireless and countless hours with me staring at the optical profilometer. Professor Chanman Park, Professor Sarath Menon, and Mr. John Mobley: I could not have completed this thesis without your support. Finally, I would like to give an overall thanks to the NPS Mechanical Engineering Department, in particular to Professor Sanjeev Sathe, Professor Claudia Luhrs, and my program advisors, Commander Porter and Commander Keller.

Last, I could not leave out my wife, Kelly, and daughters Peyton, Carsen, and Kory, who inspire me to be a better person every day through their support, character, and love. I am truly blessed!

THIS PAGE INTENTIONALLY LEFT BLANK

I. INTRODUCTION

A. MOTIVATION

AA5083 is a marine-grade 5XXX aluminum alloy with medium strength, good corrosion resistance, weldability, and a high strength-to-weight ratio [1]. Since World War II, the Navy has used aluminum and aluminum alloys as building materials for superstructures and deckhouses because of those properties [2]. High-strength aluminum alloys have one-third the density of steel with sufficient strength, which allows naval ships to be lighter, corrosion resistant, faster, and fuel efficient. Current naval applications of 5XXX alloys include CG47 cruiser class superstructures (5456-H116) and structures for both variants of the Littoral Combat Ship (LCS, 5083-H321) [2].

Despite its many benefits, 5XXX alloys can experience significant problems with stress corrosion cracking (SCC) if sensitized by prolonged thermal exposure. The CG-47 cruiser class experienced significant SCC due to high degree grain boundary sensitization. During the mid-2000s after approximately half of the expected lifespan of some of the CG-47 cruisers, significant SCC cracks were formed in areas not expected to have fatigue loading or high structural stresses. The cause was the sensitization of the aluminum alloy under a tensile stress that left areas of the aluminum superstructure susceptible to SCC. 5XXX series alloys are alloyed with magnesium to increase strength characteristics, but the magnesium level for AA5083 and AA5456 exceeds the room temperature solubility, thus leading to the potential precipitation of an intermetallic compound. Sensitization is a phenomenon in which excess magnesium migrates from the grains to the grain boundaries during exposure to elevated temperatures between 50°C and 200°C for an extended period of time [3]. The elevated temperatures result in the precipitation of β-phase (Mg_2Al_3), which is anodic compared to the nearby grain boundary regions as well as the matrix [3]. The precipitate-free grain boundary region/matrix and the β-phase precipitates form a galvanic couple that causes significant intergranular corrosion (IGC) and intergranular stress corrosion cracking (IGSCC) [4, 5].

Unfortunately for the CG-47 cruisers, the causal factors and consequences of sensitization were not fully realized until adverse effects of IGSCC occurred later in the ships' service. To mitigate the risk of SCC and understand all factors that influence the corrosion of aluminum alloys, more research needs to be done to improve repair methods on CG-47 cruisers, as well as improve manufacturing and preventative processes in projects such as the new Littoral Combat Ships (LCS, using AA5083-H116). One area of research is on the welding processes used for aluminum alloys, including friction stir welding (FSW) and gas metal arc welding (GMAW) [6]. Though these welding techniques can improve the manufacturing and repair products for aluminum alloys, the microstructural changes and residual stresses incurred must be explored to fully understand the impact of these processes to include downstream corrosion issues.

Welding causes microstructural changes to the base metal and creates residual longitudinal and transverse stresses, both of which are driving factors of SCC. Models of SCC for aluminum-magnesium alloys are necessary to continue to utilize AA5xxx alloys while mitigating their susceptibility to SCC. SCC has three factors required to occur: A susceptible material in a corrosive environment under tensile stress. All three facets of SCC need to be analyzed to verify proper modeling, and extensive research has been performed to understand the corrosion of aluminum alloys [1, 2, 3, 6, 7, and 8]. A large amount of research has been done on the sensitization of 5XXX series alloys, the corrosive environment that corrosion occurs, but little knowledge is available on the effects of stress on localized corrosion prior to a fully formed crack. The research in this thesis focused on the role of elastic stress, the orientation of the applied stress, and the degree of sensitization on the nucleation of stress corrosion cracks through localized corrosion in the alloy AA5083-H116. By looking at the role that stress plays on localized corrosion, improved manufacturing process may be found, repair practices can be improved and preventive measures can be more effective.

B. STRESS CORROSION CRACKING AND LOCALIZED CORROSION OF 5XXX ALUMINUM ALLOYS

SCC is a concern since detrimental corrosion damage can occur with little or no detection as compared to other forms of corrosion, (e.g., general or uniform corrosion that results in appreciable mass loss). However, other forms of localized corrosion are more prevalent in aluminum alloys. Pitting corrosion is the most likely form of corrosion, while crevice corrosion can form in areas of small tolerances, and exfoliation corrosion can occur on flattened grain boundary surfaces such as in cold rolled AA5083. IGSCC usually forms inside and around pit formations [1]; therefore, other localized forms of corrosion such as pitting must be analyzed with SCC to fully understand corrosion issues of aluminum alloys.

As previously mentioned, three factors are required for SCC to occur in aluminum alloys: a sensitized metal under tension in a corrosive environment (see Figure 1). SCC comes in two varieties: IGSCC and transgranular stress corrosion cracking (TGSCC). TGSCC, as its name implies, typically forms cracks through the grains of the alloy. IGSCC is more likely to occur in 5XXX series alloys due to sensitization and the precipitation of β phase, Al_2Mg_3, along the grain boundaries (see Figure 2). Aluminum alloys are marine grade and normally resistant to general and localized corrosion, but if exposed to elevated temperature for prolonged periods of time the alloy becomes sensitized. Since the β phase is more anodic than the aluminum metal matrix, a galvanic cell is formed, causing dissolution of the β phase. Cracks will then nucleate along the grain boundaries and as discussed earlier, nucleate from pits. IGSCC is related to IGC in that the kinetics of the reactions are similar and the transition from IGC usually leads to IGSCC when stress is applied [7].

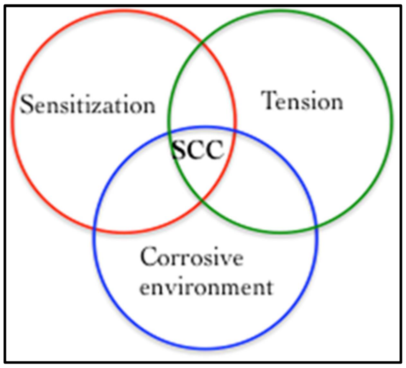

Figure 1. Venn diagram showing the requirements for SCC to occur.

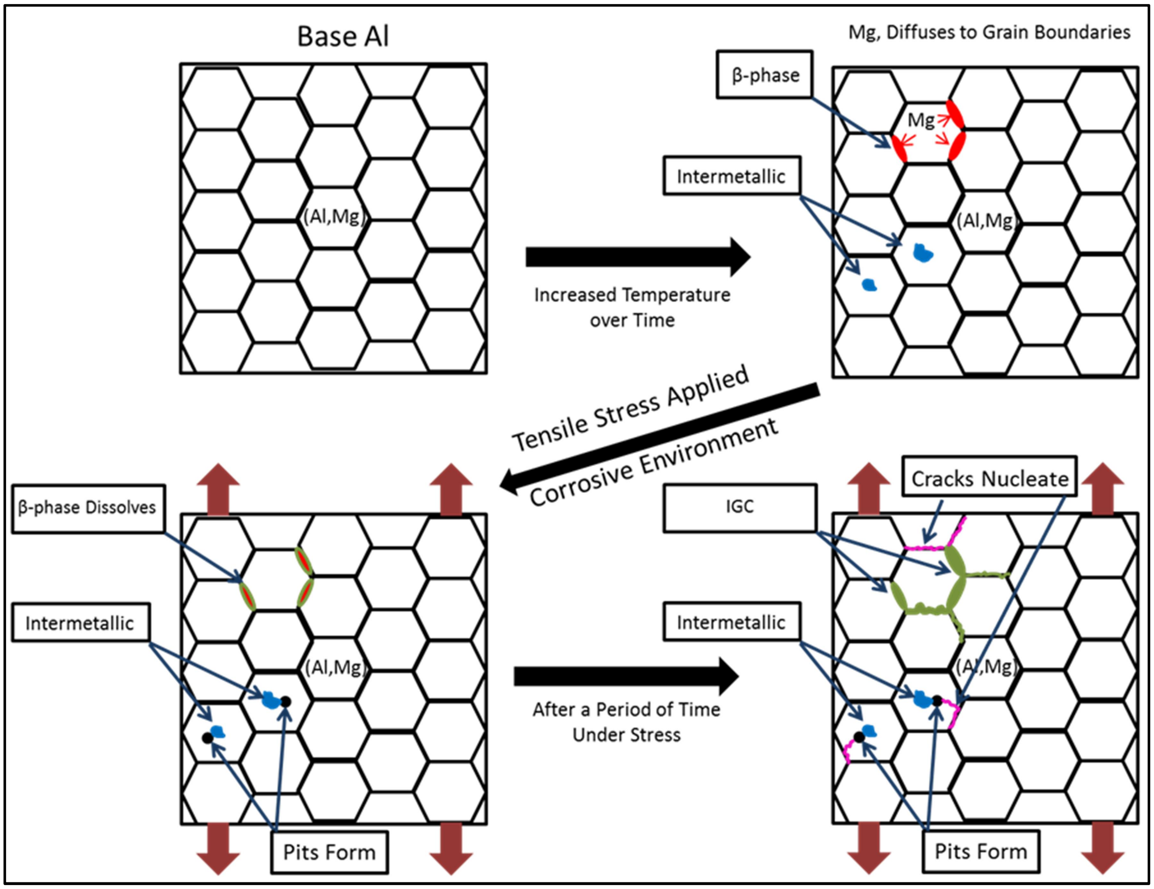

Figure 2. Schematic showing sensitization of an aluminum alloy, nucleation of localized corrosion such as IGC or pitting at intermetallic interfaces, and propagation of IGSCC from these sites, from [8].

1. Aluminum Alloy 5083-H116

Aluminum alloys are classified by the various elements added to give desired properties of the alloy. A four-digit numerical designation to classify each of the different alloys for wrought product, as defined by the Aluminum Association, is used [9]. The first digit indicates the alloy group that contains specific main alloying elements. 1XXX series alloys are primarily aluminum with a minimum Al content of 99.0%. The main alloying elements for 2XXX, 3XXX, 4XXX, 5XXX, 6XXX, and 7XXX series alloys are copper, manganese, silicon, magnesium, both magnesium and silicon, and zinc, respectively. The second digit designates the modification that was done to the original alloy. The last two digits designate the specific aluminum alloy [9]. There is also a temper designation that is given to indicate the type of mechanical and/or heat treatment that was performed on the alloy. The basic temper designations include: F (as fabricated), H (strain hardened), O (annealed), T (stable thermal heat treatment), and W (solution heat treated). The details of the classification of aluminum alloys are only important for understanding the manufacturing process, the alloying agents that are mixed in the metal, and the microstructural makeup of the alloy. Aluminum alloys in the 5XXX contain a supersaturated magnesium content, which is 3% nominal or higher [10]. They are used in conditions with temperatures no greater than 66°C (150°F) [9]. The H116 temper can be applied to aluminum alloys in the 5xxx series, where the alloy is strain hardened to meet specified levels of corrosion resistance and hardness. AA5083-H116 is strain hardened by cold rolling the alloy to a 1/8 hardness [10], making the grain microstructure anisotropic. This is an important aspect for this research and will be further discussed in the IGC and the stress section. Figure 3 shows the direction of grains with respect to the rolling direction. The following is the orientation guide for this paper:

L—Longitudinal direction parallel to the rolling direction
T—Long Transverse direction perpendicular to the rolling direction
S—Short Transverse direction perpendicular to the rolling direction

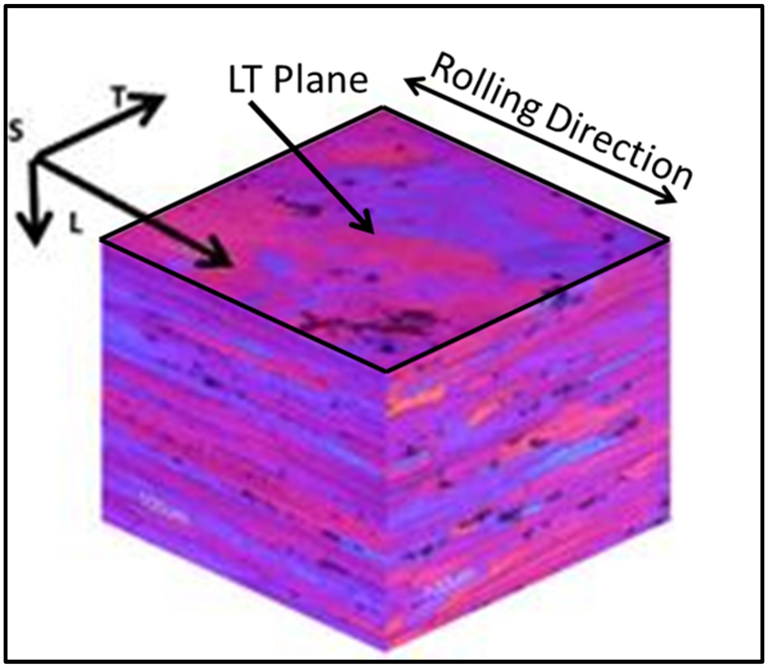

Figure 3. Orientation of grain structure with respect to rolling direction of AA 5083, from [11].

2. Sensitization of AA5083

AA5083 is considered a susceptible material to SCC when it is sensitized to the point where the β phase, Al_3Mg_2 precipitates, are nearly continuous along the grain boundaries [12]. The degree of sensitization (DoS) in aluminum alloys is a function of material (specifically, the magnesium content), grain boundary orientation, elevated temperature exposure, and time exposed to the elevated temperature. Sensitization of 5XXX series alloys can occur at as low a temperature as 40–60°C (122°F) [10]. A material's degree of susceptibility to intergranular corrosion is dependent on several variables including sensitization temperature, time at temperature, stress orientation, and type of corrosive environment [10]. The higher the temperature and the longer the metal is exposed to elevated temperatures will promote more sensitization. The ASTM G67 nitric acid mass loss test (NAMLT) is the standard test method for determining the susceptibility to intergranular corrosion of 5xxx series aluminum alloys [13]. This test measures the change in weight of samples both before and after exposure to nitric acid. The nitric acid preferentially dissolves the beta phase; thus the mass loss is representative of the amount of β phase Al_3Mg_2 in the alloy. A sample with a mass loss greater than 25 mg/cm^2 is considered susceptible to intergranular forms of corrosion [13]. The effects of sensitization can also be seen in potentiodynamic tests. Since the β phase Al_3Mg_2 is more anodic than the aluminum metal matrix and grain boundary matrix, the open circuit potential and pitting potential of the alloy will change based on DoS. Jain et al. showed that as the DoS increases, the open circuit potential (OCP) becomes substantially more negative, indicating a larger driving force for corrosion in the alloy (see Figure 4).

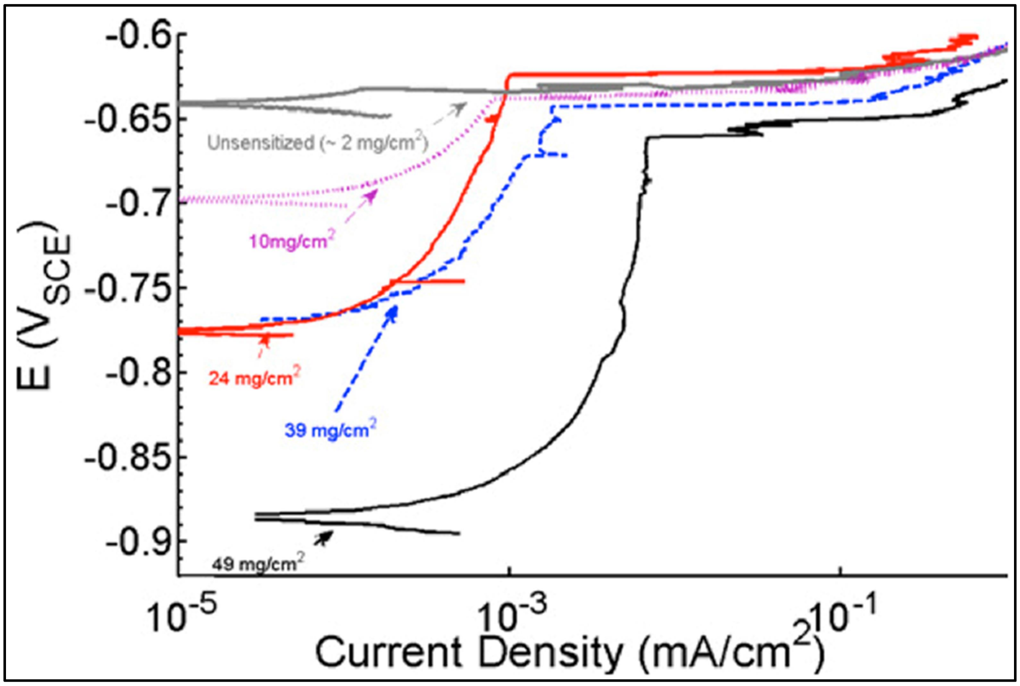

Figure 4. Polarization curves for AA5083-H131 on the LT plane at varying DoS, showing that as the DoS increases the OCP becomes more negative. The current density for a given potential also increases. DoS was measured by NAMLT, from [11].

3. Pitting Corrosion

Pitting corrosion is a highly localized form of corrosion in which cavities form on the surface of the material. These cavities, or pits, usually form due to the dissolution of aluminum matrix at an oxide film rupture. Pitting corrosion can become more severe in the presence of intermetallic precipitates where microscopic galvanic cells form between the aluminum matrix and the precipitate [5, 10, and 14] (see Figure 5). Precipitates such as β phase Al_3Mg_2 are anodic compared to the aluminum matrix, and induce dissolution of the surrounding matrix where pits nucleate [14]. N. Birbilis et al. summarized the potentials of intermetallic compounds common in aluminum alloys (Table 1). Pitting susceptibility can be related to the presence of different intermetallic precipitates in the aluminum matrix that when exposed to saltwater solutions on the surface of the alloy create a local corrosion cell. IGC can accompany the pit formations promoting larger and deeper pits [15]. IGC itself can lead to pit formation, where the anodic β-phase Al_3Mg_2 can dissolve and form elongated pits resembling cracks (see Figure 6).

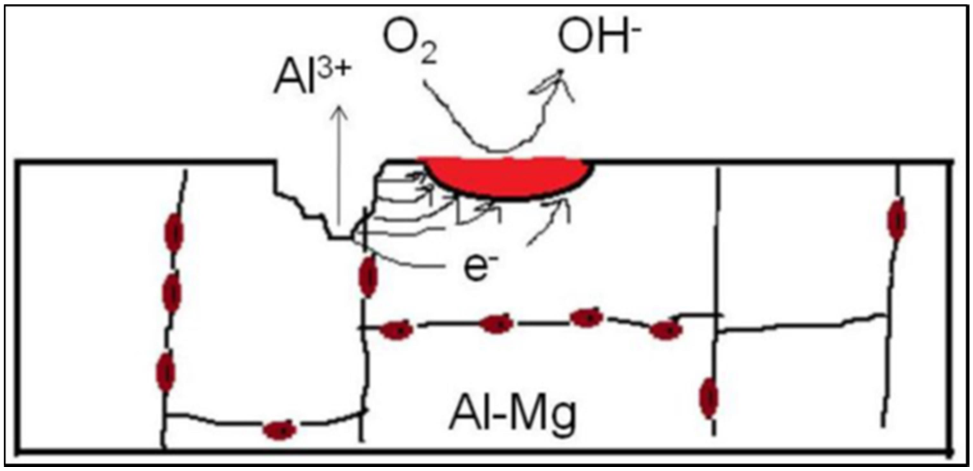

Figure 5. Cathodic pit formation and intermetallic galvanic coupling, from [1].

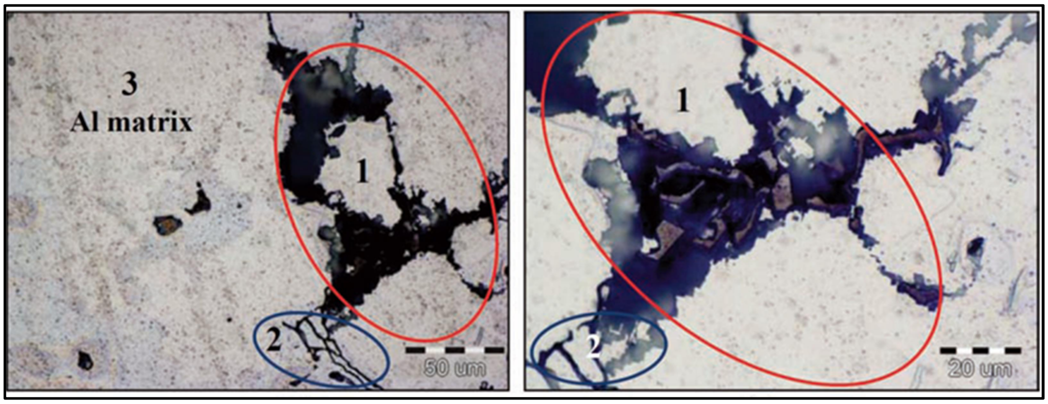

Figure 6. Pit formed from galvanic coupling between Al-Fe intermetallic particle and Al matrix (red circle), from [14].

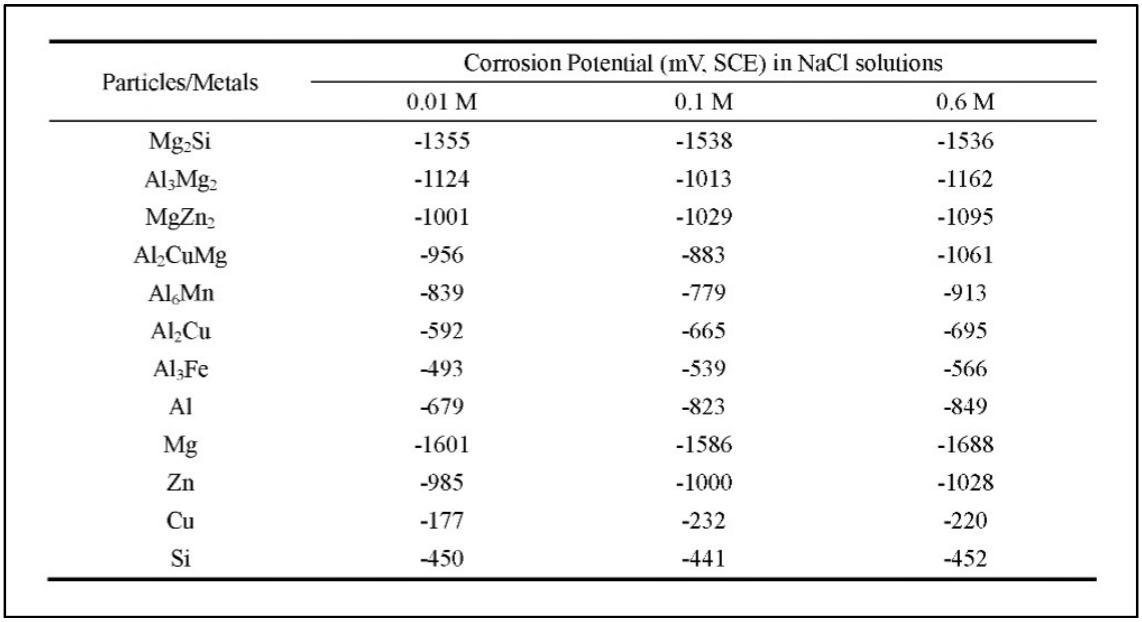

Particles/Metals	Corrosion Potential (mV, SCE) in NaCl solutions		
	0.01 M	0.1 M	0.6 M
Mg_2Si	-1355	-1538	-1536
Al_3Mg_2	-1124	-1013	-1162
$MgZn_2$	-1001	-1029	-1095
Al_2CuMg	-956	-883	-1061
Al_6Mn	-839	-779	-913
Al_2Cu	-592	-665	-695
Al_3Fe	-493	-539	-566
Al	-679	-823	-849
Mg	-1601	-1586	-1688
Zn	-985	-1000	-1028
Cu	-177	-232	-220
Si	-450	-441	-452

Table 1. Corrosion potentials for intermetallic compounds common in aluminum alloys, from [16].

A characteristic feature of pitting corrosion is the pitting potential displayed on a Tafel plot marked by a sharp increase in current density at potentials above the passive range. The pitting potential is the electrochemical potential above which pits will initiate at an observable rate. The pitting potential is sometimes referred to as the breakdown or critical potential and it is related to the localized breakdown of the oxide film. However, Gupta et al. and Cavanaugh et al., demonstrated that pit formations can still form if potential is held under the pitting potential through the formations of metastable pit formations (see Figure 7). These metastable pits can go on to form larger pit formations, or can occur in relatively large pits and continue to make it grow. Stable pit formation is the formation of pits above the pitting potential without the subsequent reformation of the passive layer. Metastable pit formation is the formation of pits with the subsequent reformation of the passive layer [17]. The instability in potentiodynamic runs (see Figure 7) and applied potentiostatic holds (see Figure 8) is usually an indication of the number of metastable pits being formed; however, metastable pits can also occur within a pit to form larger pits.

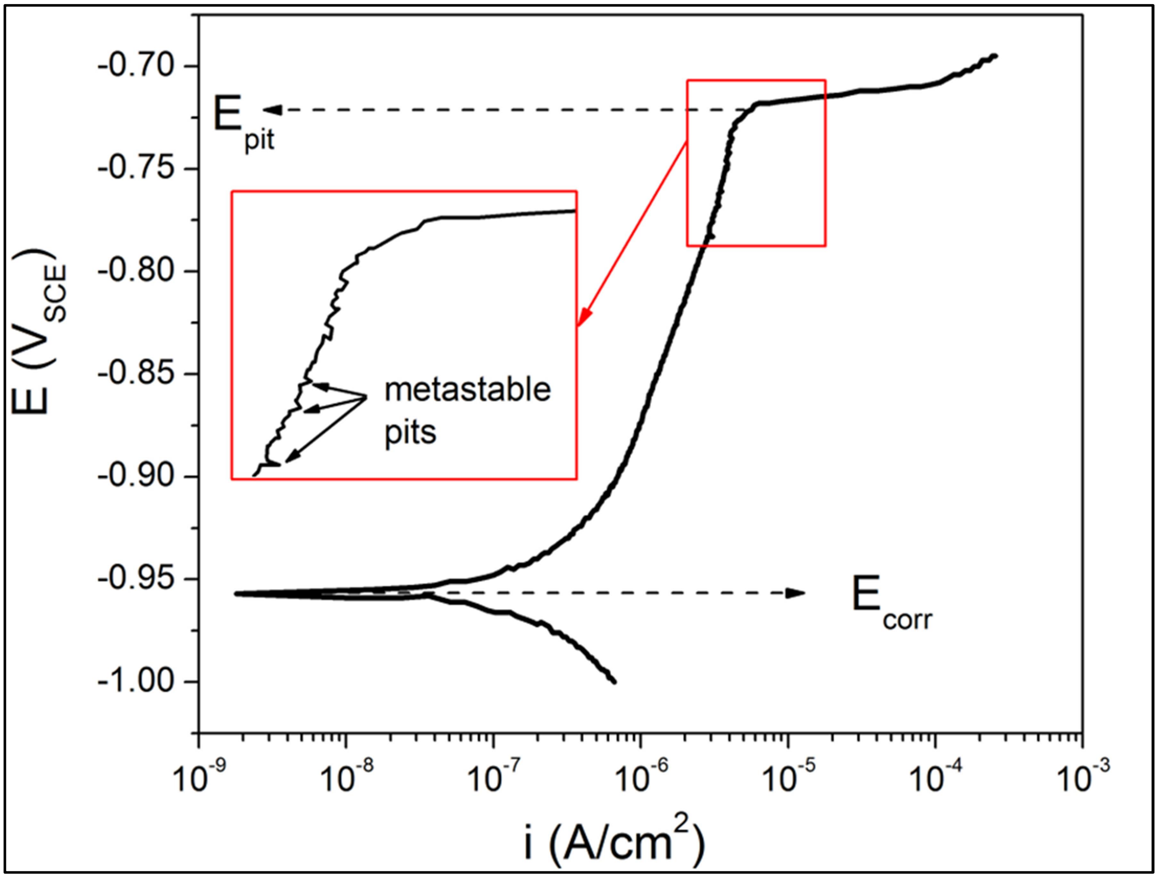

Figure 7. Potentiodynamic curve demonstrating metastable pit formation below the pitting potential, from [17].

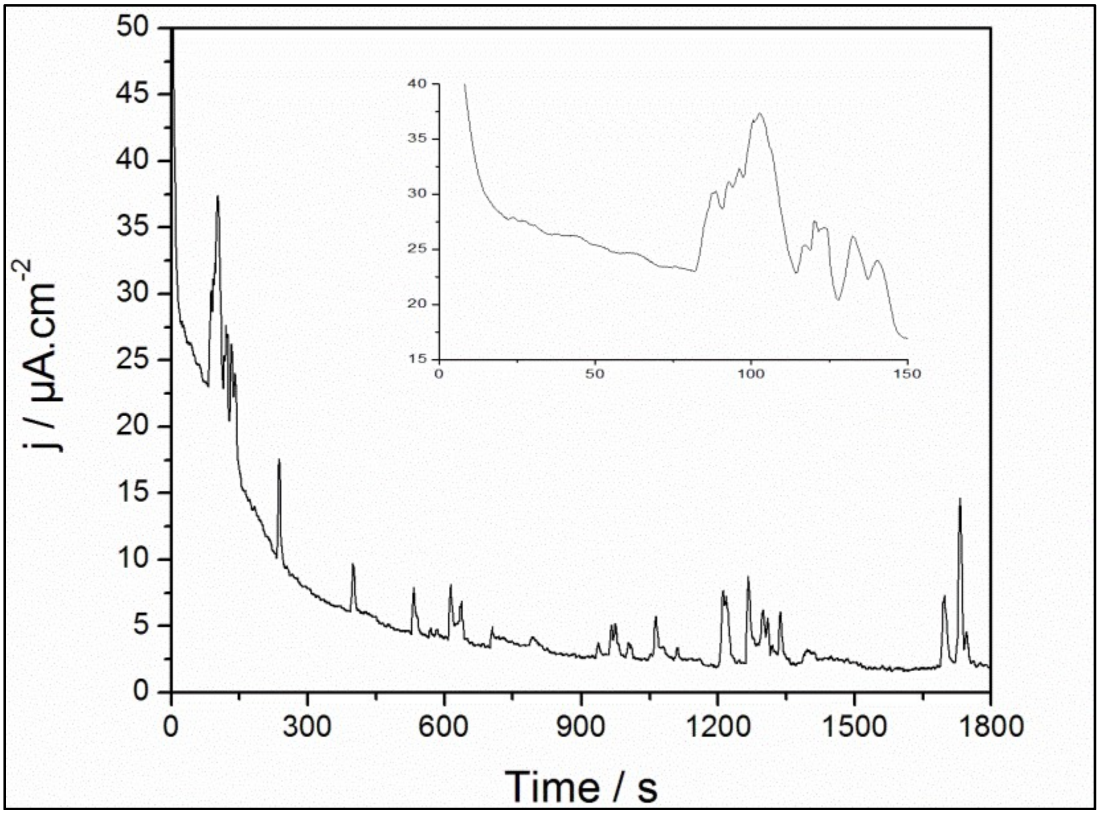

Figure 8. Potentiostatic curve of AA5083 in a deaerated NaCl solution comparing current density versus time showing metastable pit formations based on spikes occurring in the plot, from [18].

4. Intergranular Cracking

IGC is the preferential dissolution of the grain boundaries in the presence of a more anodic precipitate such as β phase Al_3Mg_2. The mechanisms of IGC are the same as IGSCC with the exception of an applied tensile stress. The presence of IGC usually leads to IGSCC once a stress is applied to a susceptible material. Work by Scully et al. showed that the grain orientation of the alloy metal played a large role in the depth of penetration of IGC in AA 5083 (see Figure 9). Sensitized AA5083 exposed to 0.6M NaCl solution under an applied voltage had significant IGC in as little as 24 hours. By changing the exposure plane (e.g., L-S, versus S-T) of the alloy in contact with the NaCl solution and the applied potential, Scully found that the ST plane with corrosion in the longitudinal direction produced the most IGC and exfoliation damage [8].

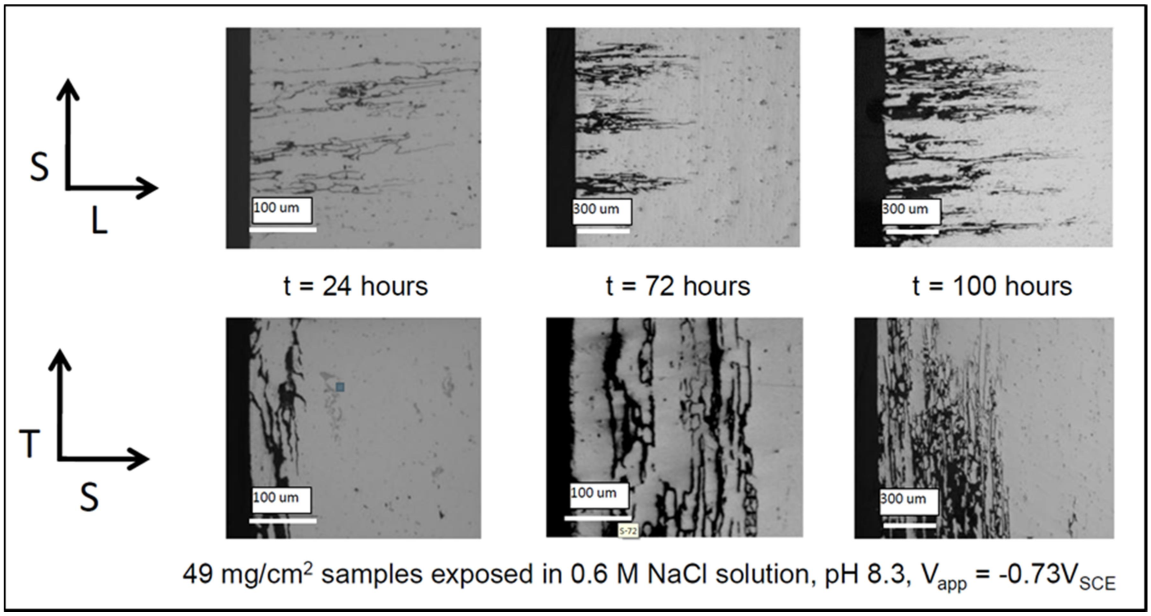

Figure 9. The Effects of Orientation on the Propagation of IGC. Top image: IGC in the ST Plane in the L direction. Bottom Image: IGC in the L Plane in the S direction, from [8].

5. Exfoliating Corrosion

Exfoliation corrosion (EFC) is a form of IGC that occurs along elongated grain boundaries in the rolling direction. The corrosion products have a larger volume than the parent metal, and whole grains may be lifted from the surface [5]. EFC is more common in 2XXX and 7XXX series alloys, but can occur in 5XXX series alloys. Exfoliation, or delamination, is addressed in work by Brosi et al., who determined that delamination in AA5456 was attributed to applied transverse stresses, which were sufficient to cause fracture along sensitized grain boundaries. Furthermore, Brosi performed interlaminar fracture toughness tests on sensitized AA5083, and found that samples failed rapidly when tested in the short transverse (ST) direction but not in the long transverse (LT) direction [19]. This result indicates that stress orientation could play a factor in localized corrosion based on the orientation of the grain boundaries.

C. ROLE OF STRESS ON CORROSION

Early work on the role of stress on corrosion in the 1960's showed that plastically deformed metals had a much higher rate of corrosion than unstressed and elastically stressed metals (Carbon steel, zone refined iron, Mo, Cu) in an acidic environment [20,21,22]. The conclusion was that stress applied above the yield stress produced a large number of dislocations with increased electrochemical activity. These dislocations increased the rate of anodic dissolution. Fouroulis and Uhlig also suggested that interstitial carbon, nitrogen, and other micro-alloyed constituents would affect the anodic dissolution be creating microgalvanic cells [20]. Furthermore, corrosion tended to be more localized as deformation increased, and corrosion levels changed with orientation of the grain boundaries. These early experiments concluded that applied stress in the plastic region had a large effect on corrosion, but the consensus was the effects caused by elastic stress were minimal.

The role that applied stress has on the effects of corrosion in aluminum alloys; specifically in the orientation that the stress is applied is still under investigation. Liu et al. measured the effects of elastic stress applied in different orientations with respect to grain microstructure on the electrochemical behavior of AA2024-T3 [23, 24]. Liu found the pitting potential to be much lower in stressed samples as compared to unstressed samples. The conclusion was that stressed samples were more susceptible to localized corrosion. Liu also found the level of applied potential changed the rate of corrosion penetration and corrosion type. AA2024-T3 had two breakdown potentials; a lower breakdown due to copper intermetallic particles, and the upper one due to the dissolution of grain boundaries (see Figure 10). Potentials held above the lower breakdown potential exhibited pitting corrosion, while samples held above the higher breakdown potential had more IGSCC. Samples held at higher potentials also had a higher corrosion penetration measured by the foil penetration technique. Liu also found that samples stressed in the LS plane had a more rapid crack penetration than the LT and unstressed L samples [23]. Again, this result indicated that stress and the orientation of the applied stress played a role in the localized corrosion of Al alloys. In a similar vein, we will relate the effects of stress applied in different orientations to AA5083-H116 sensitized at different levels. By adjusting stress levels, stress orientations, and sensitization levels, we will determine the role of applied stress and orientation on sensitized AA 5083.

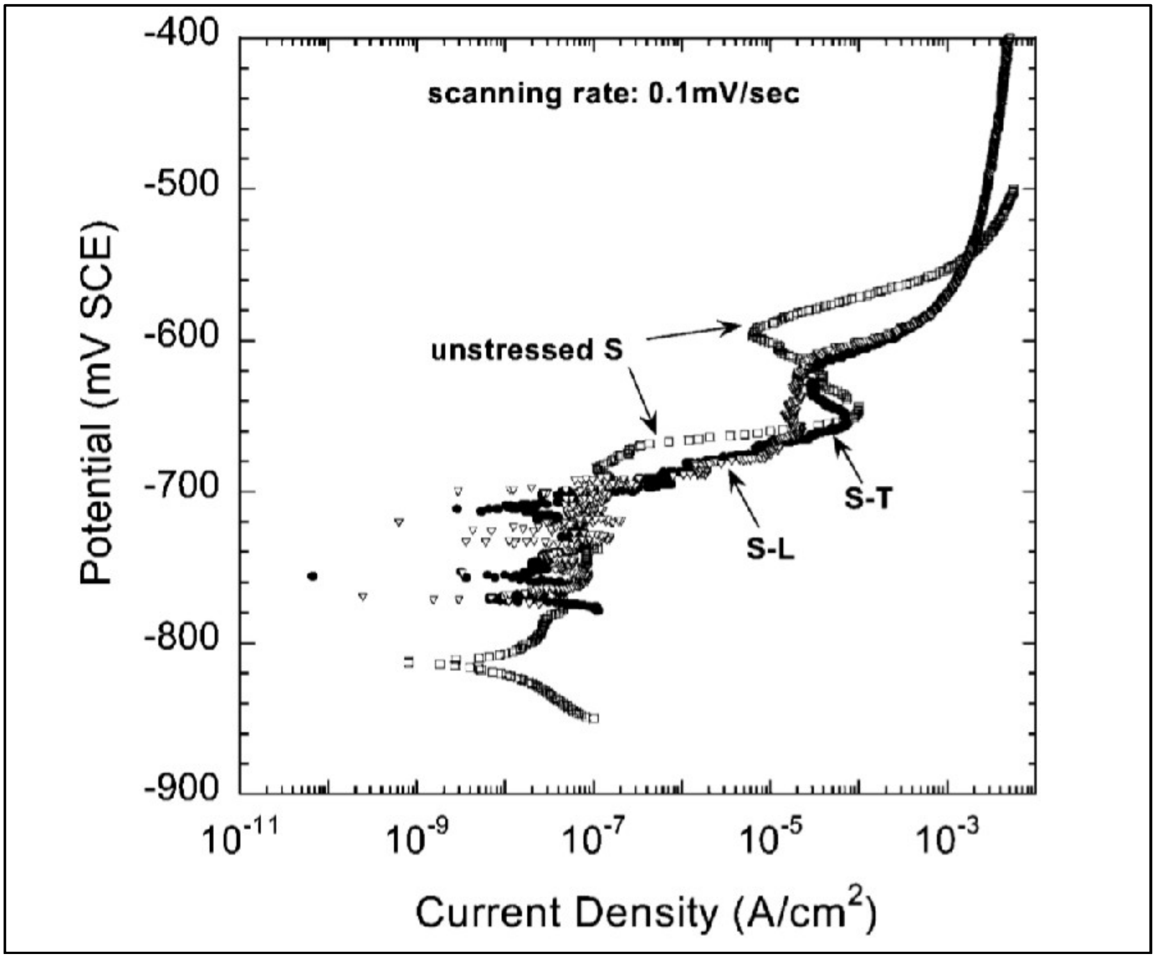

Figure 10. Anodic Polarization curves of stressed and unstressed samples. Pitting potentials changed based on stress but not on stress orientation, from [23].

D. OBJECTIVES

1. Assess the effects of applied elastic stress on the localized corrosion of AA5083-H116 during electrochemical potentiodynamic and potentiostatic testing.

We will use electrochemical testing to assess changes in localized corrosion for AA5083-H116 under applied elastic, tensile stress. We will look for changes in the open circuit potential (OCP), the pitting potential, and the rate of corrosion both under potentiodynamic and potentiostatic conditions. For the potentiostatic conditions, we will expose the samples to the stressed, corrosive environment at the open circuit potential and at an applied potential, slightly active (+35mV) to the OCP. Optical profilometry will be used to help evaluate the types of corrosion and the extent of the corrosion damage.

2. Assess the effects of microstructural orientation with regard to applied tensile stress, and sensitization on the localized corrosion of AA5083-H116.

Samples will be compared based on stress levels and orientation of applied stress to determine if the application of stress plays a role in localized corrosion of AA 5083-H116. This objective will be determined the same way that the first objective will be determined, using data from the potentiodynamic runs and analyzing optical profilometry images.

3. Implement optical profilometry to quantify localized corrosion.

As mentioned above, optical profilometry will be used to determine the types of corrosion as well as the depth and level of damage of elastically stressed AA5083-H116 exposed to 0.6M saltwater. Optical images and depth information from optical profilometry will be assessed on the ability to qualitatively and quantitatively measure the effects of SCC and localized corrosion on AA 5083-H116.

THIS PAGE INTENTIONALLY LEFT BLANK

II. EXPERIMENTAL METHODS

A. MATERIAL PROCESSING: FABRICATION AND SENSITIZATION OF TEST SAMPLES

All of the experiments in this work used AA5083-H116, 6.35 mm thick plate from ALCAN industries. The nominal composition of this plate was: 4.7 Mg, 0.9 Mn, 0.20 Fe, 0.10 Si, 0.08 Cr, 0.03 Zn, 0.03 Cu, 0 Ti [25, 26]. Samples were made by cutting 139.7 mm (5.5 in) x 50.8 mm (2.0 in) sections from this plate oriented either along the rolling direction (L orientation) or transverse to it (T orientation) (see Figure 11). The electrochemical measurements were all made on the LT plane. The samples were sensitized by placing them in a gravity convection oven at 100°C for either 7 days or 30 days. The sensitization level was measured at Naval Surface Warfare Center Carderock Division using the ASTM-G67 procedure, which involves measuring the mass loss of the specimens after a 24 hour exposure to concentrated nitric acid in a 30°C bath. The samples were stressed at stress levels of 100MPa (medium stress-M) or 200MPa (High Stress-H). The sample matrix is listed in Figure 11. The naming convention follows as orientation-sensitization level-stress level (e.g., L-7-H), would be plate oriented along rolling direction with 7 days at 100°C sensitization, tested at a stress of 200 MPa.

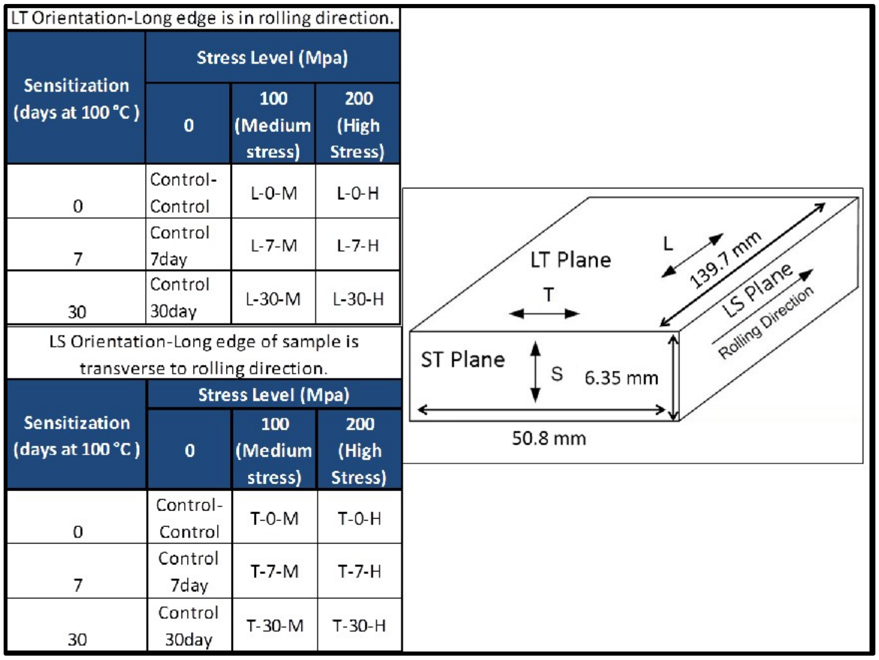

LT Orientation-Long edge is in rolling direction.

Sensitization (days at 100 °C)	Stress Level (Mpa)		
	0	100 (Medium stress)	200 (High Stress)
0	Control-Control	L-0-M	L-0-H
7	Control 7day	L-7-M	L-7-H
30	Control 30day	L-30-M	L-30-H

LS Orientation-Long edge of sample is transverse to rolling direction.

Sensitization (days at 100 °C)	Stress Level (Mpa)		
	0	100 (Medium stress)	200 (High Stress)
0	Control-Control	T-0-M	T-0-H
7	Control 7day	T-7-M	T-7-H
30	Control 30day	T-30-M	T-30-H

Figure 11. Sample matrix and dimensions for the L orientation sample.

All samples were either ground or ground and polished using the Buehler Automet 2. Samples were taped to the sample holder using 3M heavy duty double sided tape due to the size of the samples.

Potentiodynamic samples were ground to remove the passive oxide layer using the following procedure:

- Ground using 320 grit silicon carbide paper, Buehler Automet 2 settings. Speed: 120 RPM. Force: 6 lbf. Time: 20 minutes. Lubricant and coolant: water.

- Ground using 1200 grit silicon carbide paper, Buehler Automet 2 settings. Speed: 120 RPM. Force: 6 lbf. Time: 30 minutes. Lubricant and coolant: water.

Potentiostatic samples were polished for confocal and optical microscopy using the following procedure:

- Ground using 320 grit silicon carbide paper, Buehler Automet 2 settings. Speed: 120 RPM. Force: 6 lbf. Time: 15 minutes. Lubricant and coolant: water.

- Ground using 1200 grit silicon carbide paper, Buehler Automet 2 settings. Speed: 120 RPM. Force: 26.7N (6 lbf.) Time: 30 minutes. Lubricant and coolant: water.
- Ground using 2400 grit silicon carbide paper, Buehler Automet 2 settings. Speed: 120 RPM. Force: 26.7N (6 lbf.) Time: 30 minutes. Lubricant and coolant: water.
- Ground using 4000 grit silicon carbide paper, Buehler Automet 2 settings. Speed: 120 RPM. Force: 26.7N (6 lbf.) Time: 30 minutes. Lubricant and coolant: water.
- Polished using black foam pad with Buehler Metadi monocrystalline diamond 3 µm oil-based suspension, Buehler Automet 2 settings speed: 120 RPM force: 26.7N (6 lbf.), time: 30 minutes, lubricant: water.
- Polished using black foam pad with Buehler Metadi monocrystalline diamond 3 µm oil-based suspension, Buehler Automet 2 settings speed: 120 RPM force: 17.8N (4 lbf.), time: 30 minutes, lubricant: water.
- Polished using black foam pad with Buehler Metadi monocrystalline diamond 1 µ oil-based suspension, Buehler Automet 2 settings. Speed: 120 RPM. Force: 26.7N (6 lbf.) Time: 30 minutes. Lubricant: water, then rinsed with distilled water.
- Polished using black foam pad with Buehler Metadi monocrystalline diamond 1 µ oil-based suspension, Buehler Automet 2 settings. Speed: 120 RPM. Force: 17.8N (4 lbf.) Time: 30 minutes. Lubricant: water.

1. Nitric Acid Mass Loss Test

Two samples from each sensitization level were prepared and tested in accordance with ASTM G67 Nitric Acid Mass Loss Test [13]. All mass loss measurements were performed at Naval Surface Warfare Center Carderock. The test is performed by measuring the surface area of the sample and placing the sample in a nitric acid bath for 24 hours. The sample is weighed before and after the nitric acid bath, and the difference in mass is the mass loss is measured in mg/cm^2. The NAMLT is the standard test to determine a materials susceptibility to sensitization. Samples with mass losses less than 15 mg/cm2 are considered intergranular-corrosion resistant, while mass losses greater than 25 mg/cm^2 are considered highly susceptible [13].

B. ELECTROCHEMICAL CELL SETUP AND EXPERIMENTS

1. Bend Rig

The four point bending apparatus was designed in accordance with ASTM-G39 (see Figure 12). The bend rig was made of 316 stainless-steel and utilized #10 stainless steel screws with 32 threads per inch to apply stress to the aluminum coupons (see Figure 13).

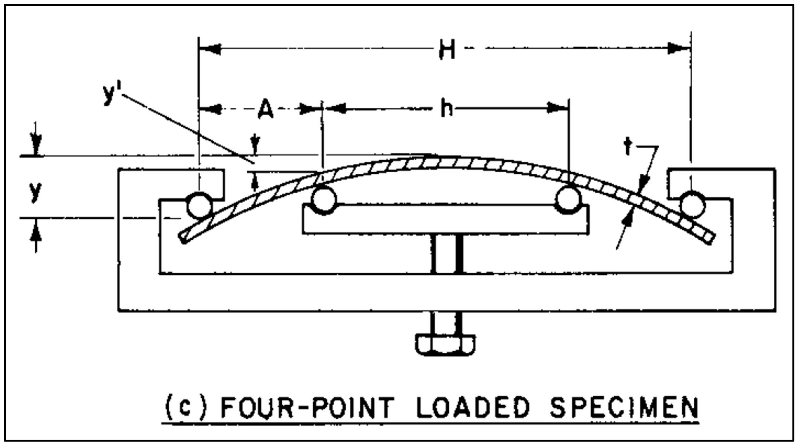

Figure 12. Four-point bend rig schematic from ASTM-G39, from [25].

Figure 13. Photograph of stainless steel 4-point bending rig used to apply elastic stress to aluminum plate samples, from [8].

The stress versus screw turn graph in Figure 14 shows the calibration used to apply the proper stress to the samples in the bend rig via the displacement screws. This calibration and its data can be found in the thesis work of B.E. Scott [8].

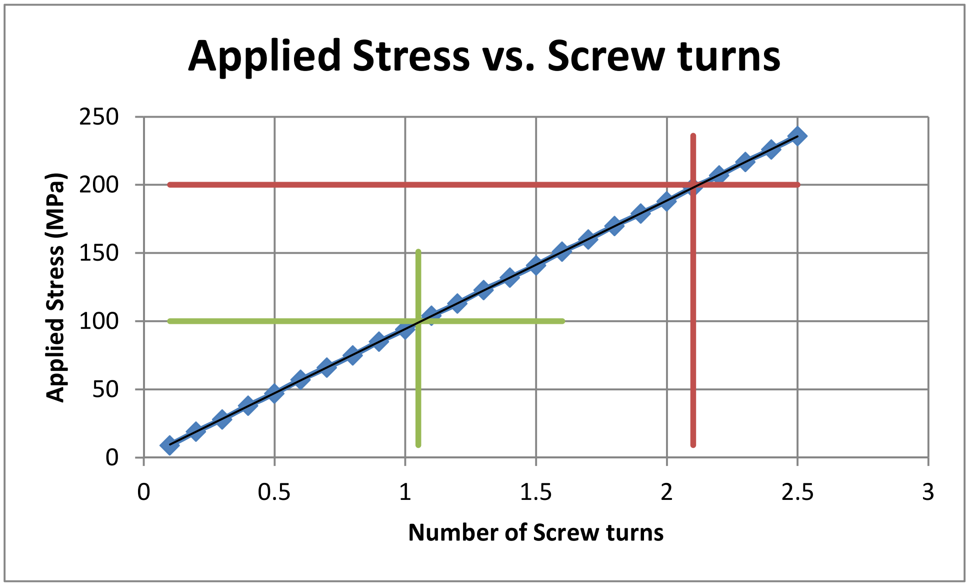

Figure 14. Photograph of stainless steel 4-point bending rig used to apply elastic stress to aluminum plate samples. (Bottom) Stress-strain data based on displacement and screw turns calculations, data obtained after [8]. The red line is the number of turns to apply 200MPa, and the green line is the number of turns to apply 100 MPa to the samples.

Screw Turns	Displacement (cm)	Stress (ksi)	Stress (Mpa)
1.125	0.09	15.03	104
2.125	0.17	28.7	198

Table 2. The two levels of stress applied to the samples during experimentation and the screw turns necessary to apply these stresses.

2. Three Electrode Cell Setup

The ground and polished samples were put into the bend rig, with the saltwater exposed side of the sample in tension. Each sample was exposed to an applied stress by the bend apparatus of approximately 100 MPa or 200 MPa. Screws were turned until the tensile stress on the top surface reached the desired level. Non-conductive plastic cups of 50 mm in diameter were sealed to the surface of the plate using extra strength 3M double sided tape. A 6 mm diameter hole (exposed surface area of 0.283 cm^2) was punched through the tape to control the aluminum plate exposed area to aerated, 0.6 M NaCl, synthetic saltwater (pH was adjusted to 8.3 using 0.1M NaOH) while under applied elastic stress (see Figure 15). Gamry Framework and Echem Analyst software was used to perform potentiodynamic and potentiostatic testing and analysis on the samples under stress. A tri-electrode cell (see Figure 16) was created by using the plate as the working electrode (WE) with a Fisher Scientific Accumet glass body Ag/AgCl mercury free standard reference cell as the reference electrode (RE) and a graphite rod counter electrode (CE). The bend rig, aluminum sample, and three electrode cell was placed into a Faraday cage to prevent stray voltages interfering with the electrochemical experiments. The Faraday cage consisted of a non-conductive container wrapped in heavy duty aluminum foil.

Figure 15. Top view of cup mounted to top of sample with double-sided tape. The area exposed to saltwater is punched through the tape.

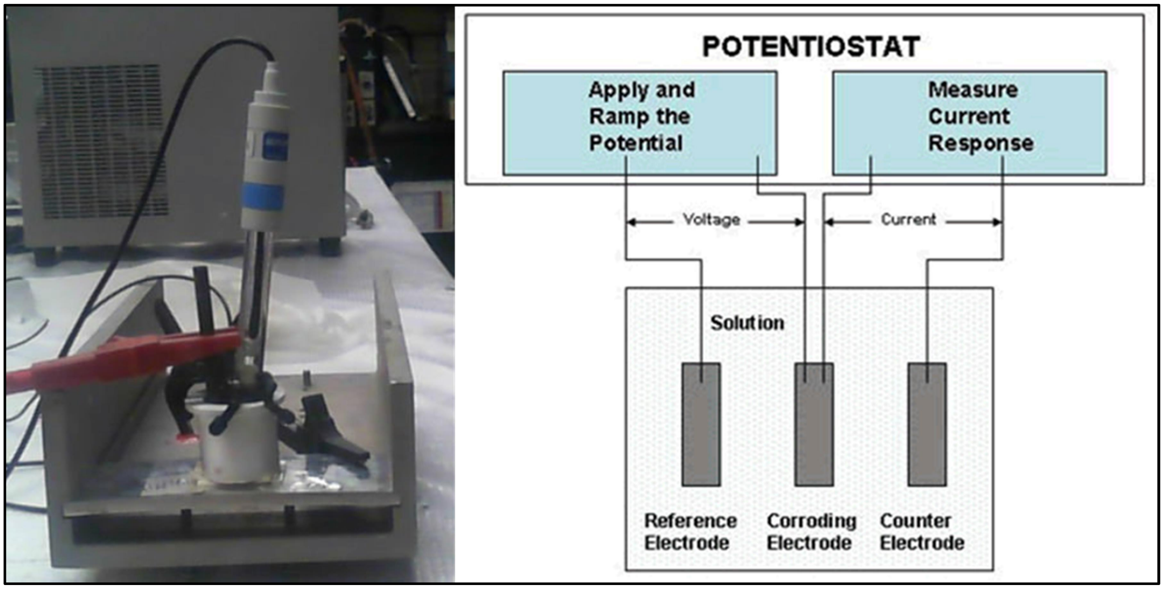

Figure 16. (Left) Photograph of bend rig with three-electrode cell used for polarization experiments. (Right) Schematic of three-electrode cell from [25].

3. Electrochemical Experiments

All electrochemical experiments were performed and analyzed using Gamry Framework and Echem Analyst software. Potentiodynamic testing was used to determine the open circuit (OCP) and pitting potentials as a function of sensitization and stress level. The system was allowed to equilibrate at the OCP for 12 hours at room temperature (63–68°C) prior to starting the potential scan. The potential scan started -30 mV below the OCP and then increased at a rate of +0.1 mV/second until a corrosion current density of 1 mA/cm^2 was reached. In potentiostatic tests, the samples were held for 72 hours at either the OCP or at +35 mV above the OCP while under varying levels of stress. All measurements were made nominally at room temperature.

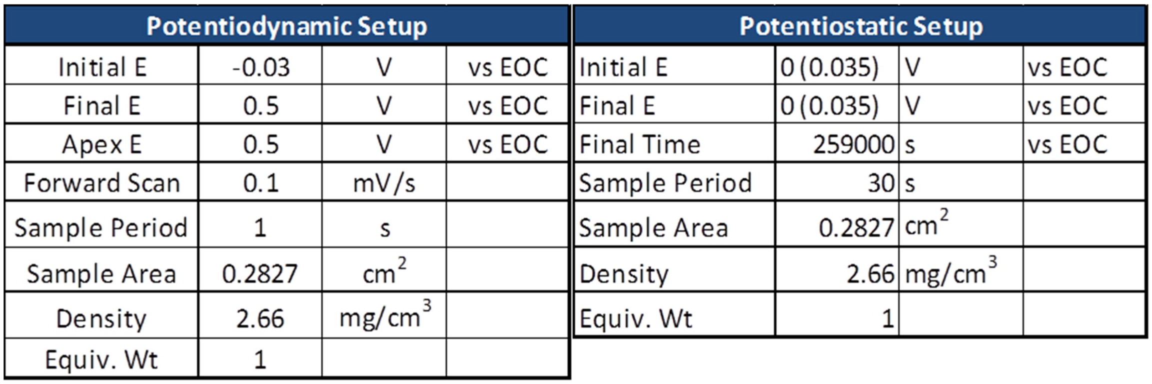

Potentiodynamic Setup			
Initial E	-0.03	V	vs EOC
Final E	0.5	V	vs EOC
Apex E	0.5	V	vs EOC
Forward Scan	0.1	mV/s	
Sample Period	1	s	
Sample Area	0.2827	cm^2	
Density	2.66	mg/cm^3	
Equiv. Wt	1		

Potentiostatic Setup			
Initial E	0 (0.035)	V	vs EOC
Final E	0 (0.035)	V	vs EOC
Final Time	259000	s	vs EOC
Sample Period	30	s	
Sample Area	0.2827	cm^2	
Density	2.66	mg/cm^3	
Equiv. Wt	1		

Table 3. Gamry Framework potentiodynamic and potentiostatic experimental setup parameters.

C. MICROSCOPY

The degree and distribution of localized corrosion was measured by a combination of optical and confocal microscopies using the Zygo NewView 7100 optical profilometer with MetroPro software (see Figure 17). Optical profilometry scans (image intensity maps) and depth images were taken of the exposed surfaces area and the whole exposed surface area image was “stitched” together to form one image. The double sided tape on the sample allowed for only the exposed surface area of the sample to be scanned. Light intensity of the scan was adjusted based on the reflectivity of the sample surface. Dual light sources were required for the corroded surfaces based on the non-reflective nature of the corrosion products and the depth of corrosion damage. The higher light intensity allowed for the corrosive areas and the large pits to be scanned, while the lower light intensity was used for the areas with high reflectivity. The Dual Light Stitch program built in MetroPro software compared the high and low light scan and automatically used the best image areas from each scan to produce the overall stitched image. Black areas in the scans indicated that no data was obtained from that area. The intensity image map is the stitched optical image at 100x magnification. Sample orientation was scanned in accordance with Figure 18.

Optical profilometry experiments were conducted before and after electrochemical tests. Image intensity maps and surface depth images were obtained of the exposed surfaces at the two 72-hour potential holds. Images obtained before electrochemical exposure were taken as a reference point to compare with samples after corrosion damage. Areas of corrosion on the optical images are seen as darker areas, whereas lighter areas indicate the areas of the surface with little or no damage. Surface depth images started at -1µm since the samples were polished to 1µm. The assumption was that anything surface features that occurred at a depth of -1 µm or greater were due to corrosion. Depth scales for the surface depth images were then varied to determine the type of corrosion as well as the depths to which the corrosion penetrated. Black areas of the surface depth images are a result of no data collected in that area due to the lack of reflected light.

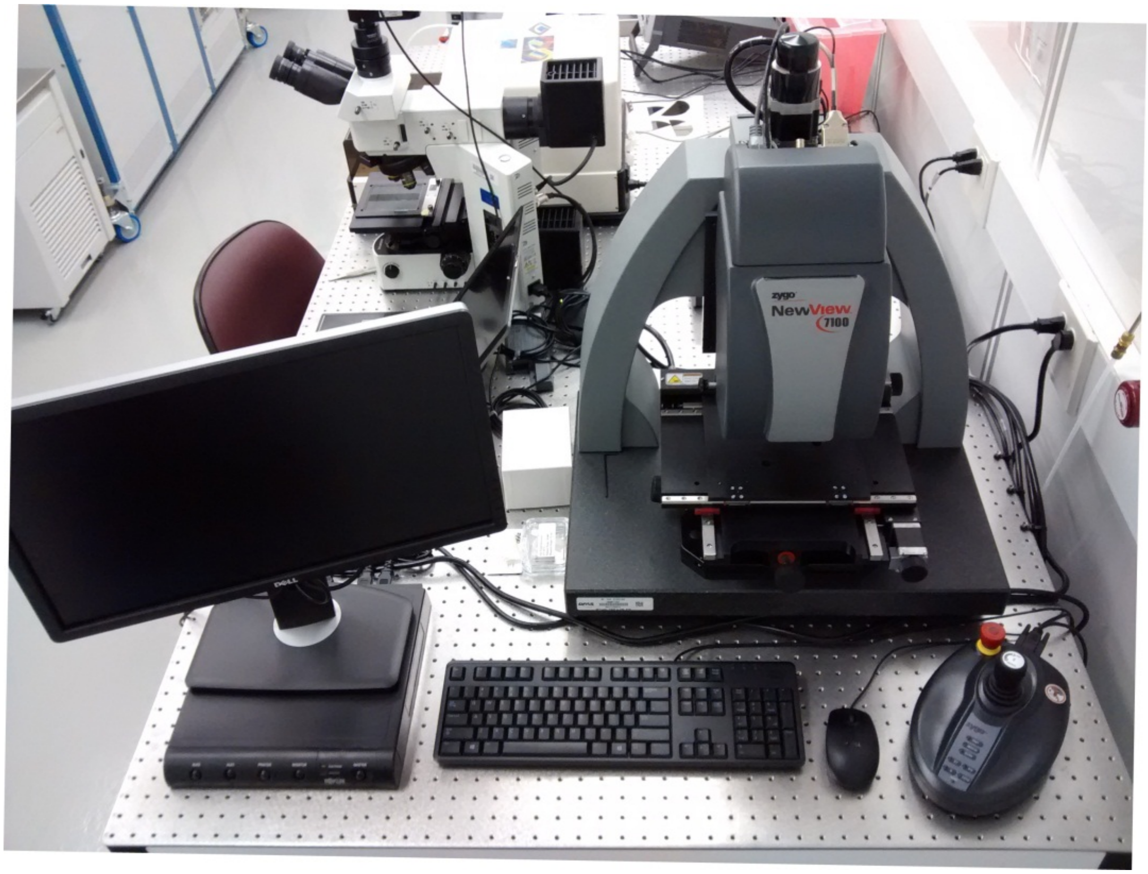

Figure 17. Optical Profilometer Zygo NewView 7100 with MetroPro software.

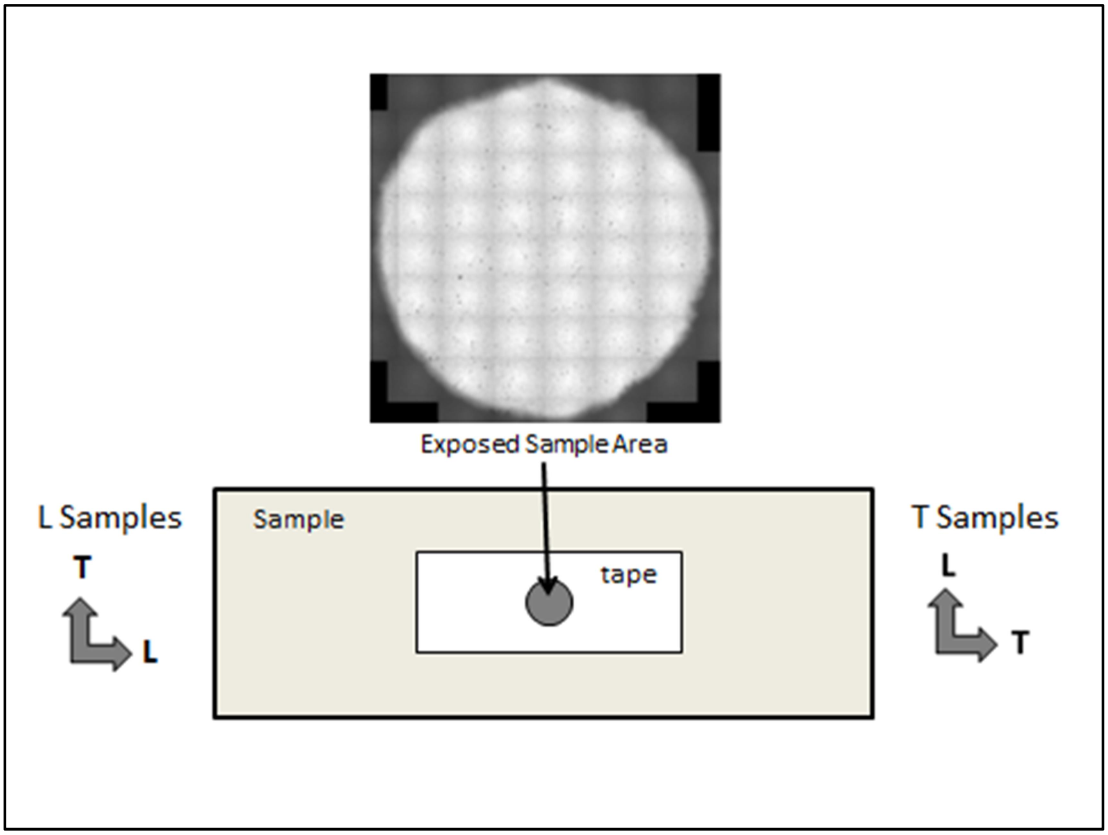

Figure 18. Orientation of samples as they were scanned with the optical profilometer. Tensile direction was left to right in all images.

Depth of the corrosion damage was determined by taking the stitched depth images from the profilometer and changing the depth scale using a color spectrum (see Figure 19). At the top of the scale, a pink color indicated that the surface area was above the depth of the scale. A dark blue color indicated the depth of the surface area was below the scale. The lowest depth of each sample caused by corrosion damage was found by changing the scale until all depths indicated a pink color. A black color indicated no data was obtained for the given area. All other colors show surface areas reside in the given depth range.

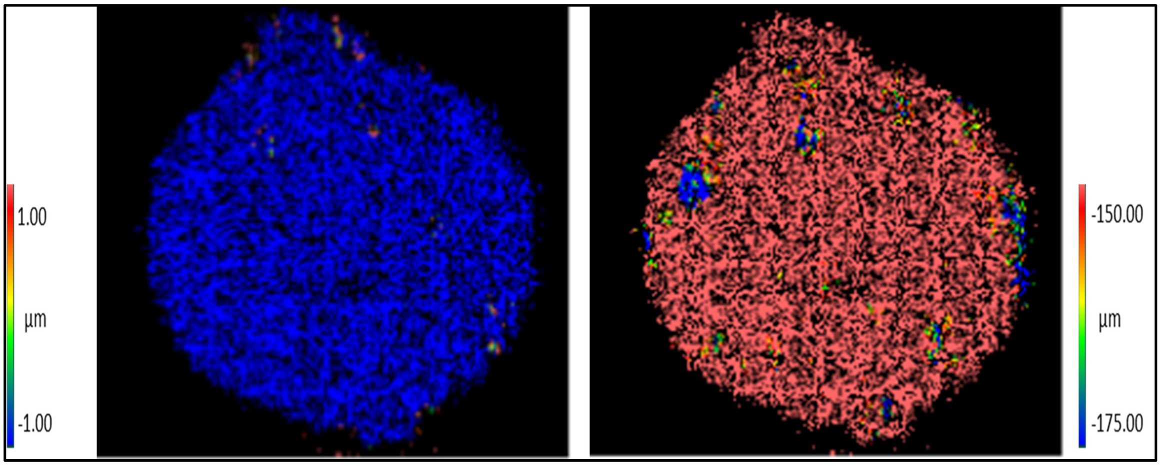

Figure 19. Profilometer depth scan of the same area on two different depth scales.

D. NITRIC ACID MASS LOSS TEST

NAMLT results performed in accordance with ASTM 67 at Naval Surface Warfare Center Carderock were used to ensure the electrochemical experiments were being performed on samples at the appropriate DoS (Table 4). The unsensitized samples were in the expected range of unsensitized aluminum (nominally less than 15 mg/cm2, while the 7-day sensitized and the 30-day sensitized samples fell into the expected 25–75 mg/cm2 [12]. The sensitization levels for the 7-day and 30-day sensitized materials were higher than in previous work such as Scully et al. [13], due to a difference in temper, H-116 versus H-131

	Days of Sensitization at 100°C					
	0 days	0 Days	7 Days	7 Days	30 Days	30 Days
Mass Loss (mg/cm^2)	7.19	7.51	44.83	44.38	53.06	55.35
Ave. Mass Loss (mg/cm^2)	7.35		44.61		53.20	

Table 4. ASTM G67 results performed by Naval Surface Warfare Center Carderock.

E. POTENTIODYNAMIC TESTING

The electrochemical response of the unstressed control samples showed a clear and expected increase in activity based on DoS (see Figure 20). The 30-day control sample was the least noble while the unsensitized control sample was the most noble. The 7 day control sample fell between the other two samples. Differences in pitting potentials and current density stability between the control samples were also observed based on DoS. The unsensitized control sample had no distinguishable pitting potential, while the sensitized control samples had a distinct pitting potential that was easier to recognize as DoS went up. The current density for the 30 day control sample had less "noise" or instability during the potentiodynamic scan as compared to the 7 day control and unsensitized control samples.

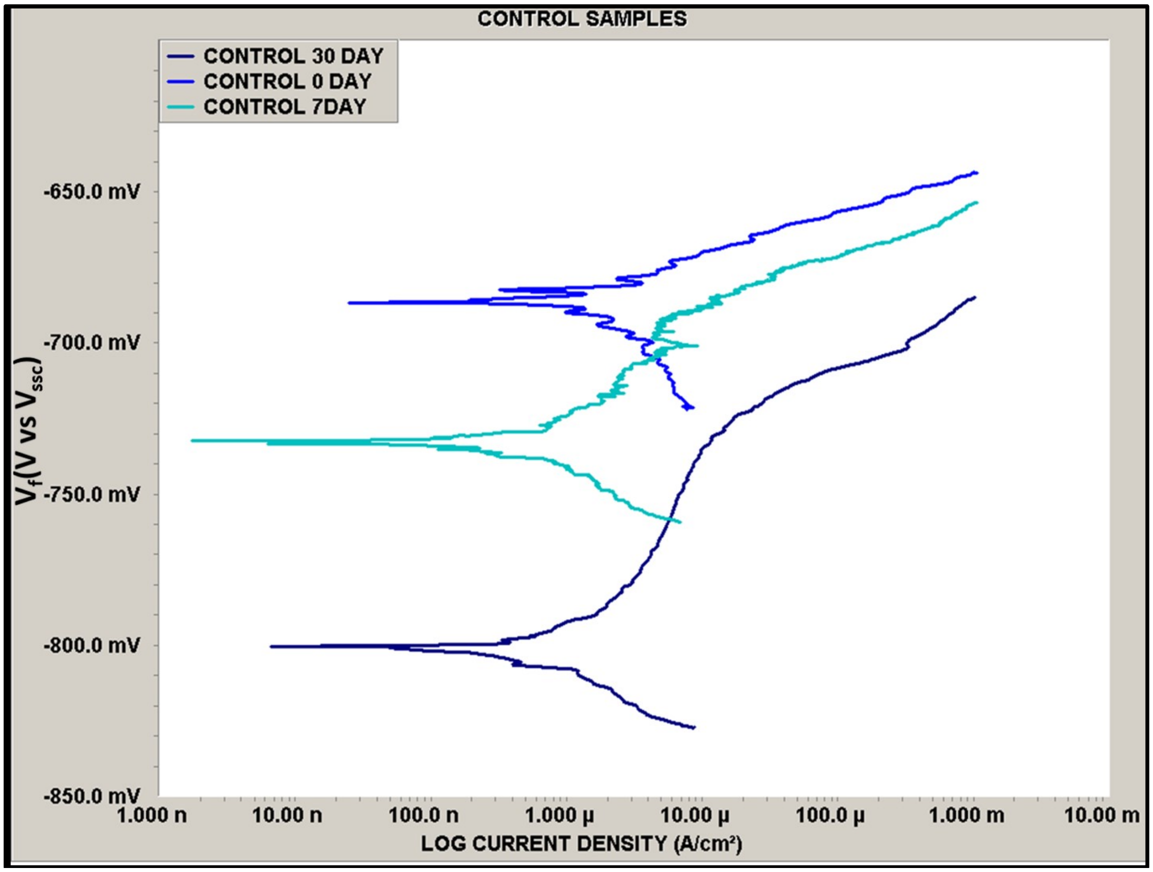

Figure 20. Potentiodynamic scans of samples at different sensitizations with no stress applied.

Unsensitized samples exposed to stresses in different orientations had a similar OCP value, but a different slope on the anodic branch of the Tafel plot. (see Figure 21) The orientation of the stress appeared to affect the corrosion rate, determined by comparing differences in log current density at a given potential. For example, current density for the three samples measured at a potential of 653mV (the average OCP for the three samples plus 35mV, Table 5) showed the T-0-H sample had the higher current density compared to the L-0-H sample and the control sample. This is a possible indication that the orientation of the stress plays a role on localized corrosion. A pitting potential was not clearly determined for the three unsensitized samples, thus general corrosion and IGSCC were expected as the main form of corrosion, with the T-0-H sample expected to have the highest degree of corrosion damage followed by the L-0-H sample and then the control sample.

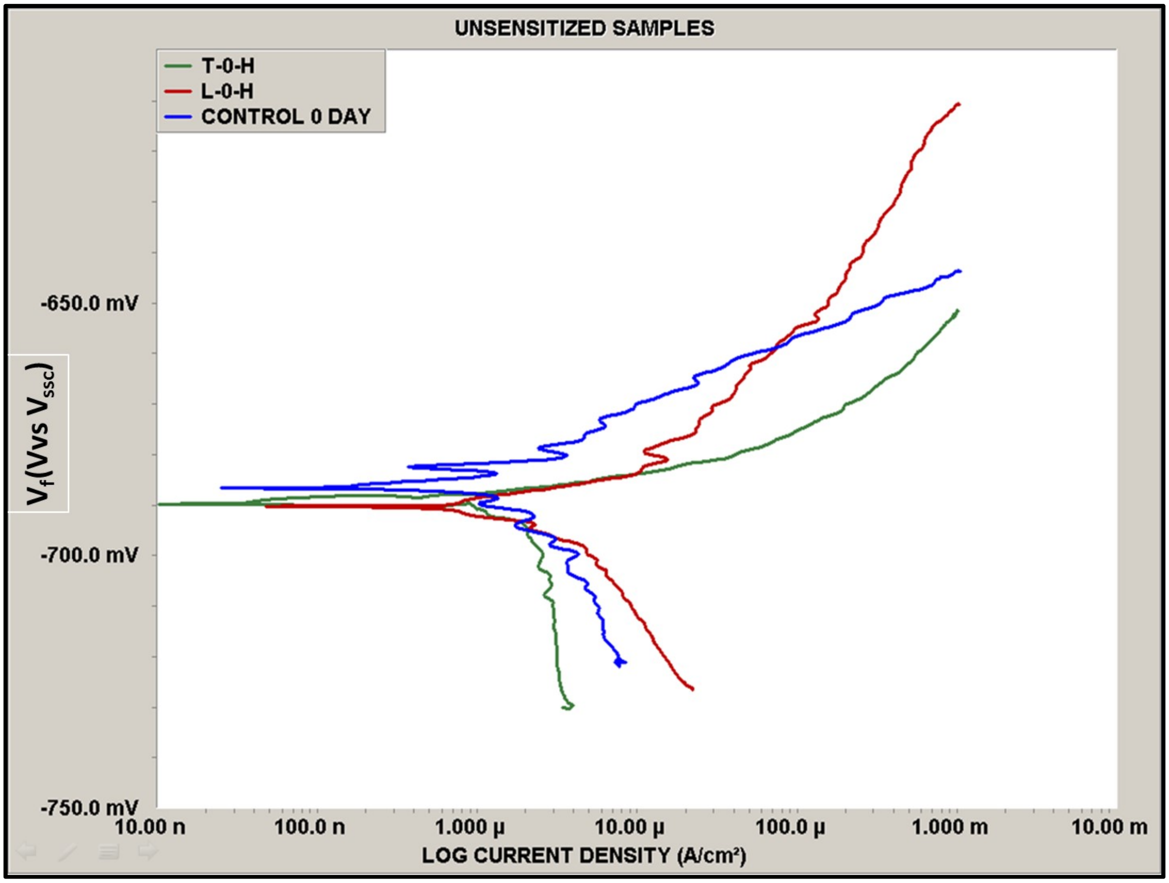

Figure 21. Potentiodynamic scans for unsensitized samples with 200MPa tensile stress applied in the longitudinal and transverse directions.

These samples were compared to the unsensitized control sample.

Current Density at Average Applied Voltage	
Sample	Current Density(μA/cm2)
Control 0 Day	210
L-0-H	136
T-0-H	904

Table 5. Current density recorded at a potential of the average applied voltage calculated using the OCP of the unsensitized samples (see Figure 21, -688mV) +35mV (-653mV).

Applying a stress to the sensitized samples changed the electrochemistry by shifting the OCP to be less negative in comparison to unstressed samples with the same sensitization level. The control 7-day sensitized sample had a more active OCP (-733.1mV) than the L and T stressed 7 day samples (-717.5mV, -712.4mV, respectively), and the difference between the two stressed samples was minimal (see Figure 22). The orientation of the applied stress played no role in changes to the electrochemistry shown in the potentiodynamic measurements. This trend was also seen on the 30-day sensitized samples (see Figure 23). Furthermore, the L-30-M sample showed that the level of stress shifted the OCP less compared to the higher stress.

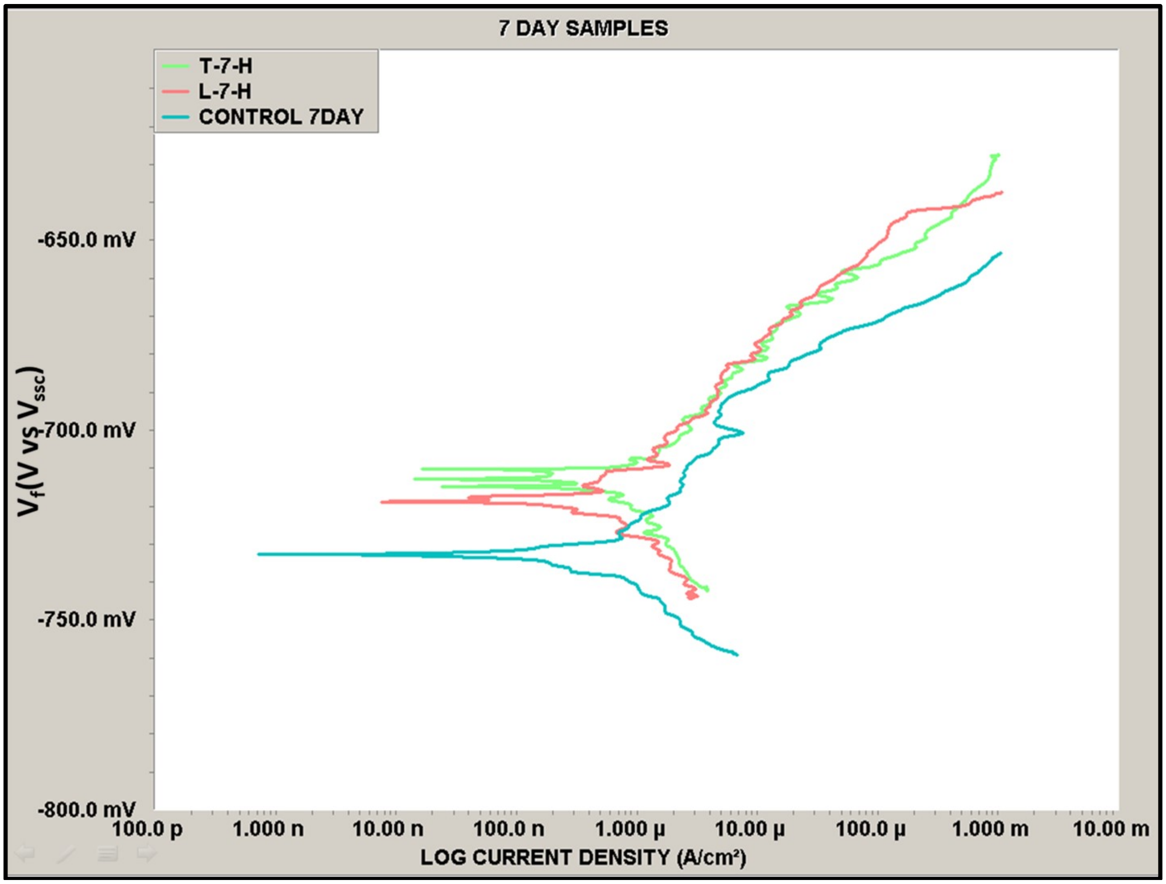

Figure 22. Potentiodynamic scans for 7 day sensitized samples with 200MPa tensile stress applied in the longitudinal and transverse directions. These samples were compared to the 7-day control sample.

While the OCP can be seen shifting based on applied stress for the 7 day and 30 day control samples, the pitting potential of the 30 day sensitized samples are relatively close to each other (see Figure 23). Therefore, as OCP was less active for the stressed 30 day sensitized samples, the difference between the OCP and the pitting potential, or the passivity range, was smaller compared to the control 30 day samples (Table 6). The L-30-M pitting potential was not determined.

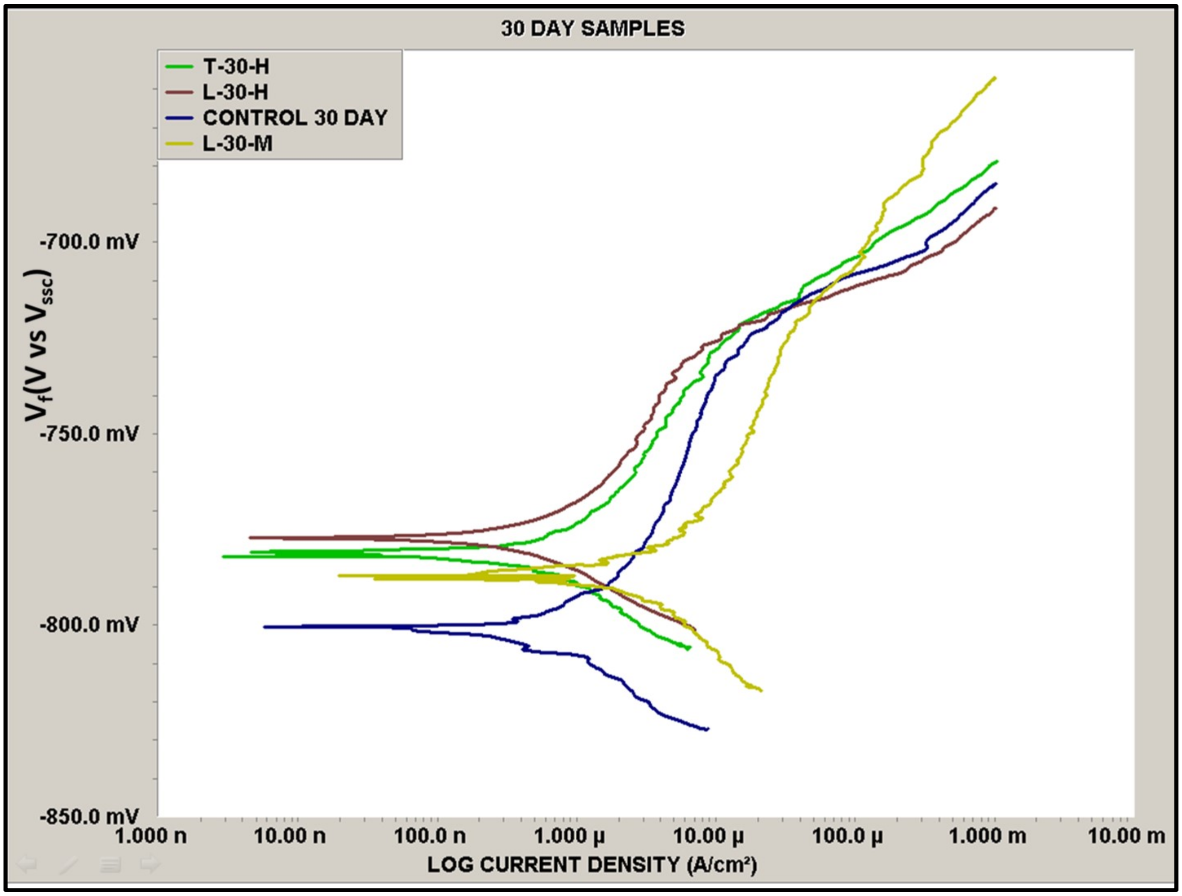

Figure 23. Potentiodynamic scans for 30 day sensitized samples with 200MPa tensile stress applied in the L and T directions and 100MPa applied in the L direction. These samples were compared to the 30 day control sample.

OCP hold Samples	OCP (mV)	Pitting Potential (mV)	Passive Range (mV) abs[OCP-Epit]	Type of Corrosion	Deepest Measured Corrosion Depth(µm)
Control Control	-687	not discernable	N/A	pitting	-5
T-unsensitized 200MPa	-689	not discernable	N/A	general	-72
L-unsensitized 200MPa	-690	not discernable	N/A	general & pitting	-78
30 Day Control	-800	-734.1	65.9	pitting	-53
T-30 Day 200MPa	-781	-728.6	52.4	pitting	-59
L-30 Day 200MPa	-777	-733.2	43.8	pitting	-33

Table 6. Comparison of OCP potential hold samples and their OCP values, pitting potentials, passive range, corrosion type, and deepest measured corrosion penetration.

A comparison of samples at the highest level of stress with varying DoS again showed that DoS was the biggest factor on electrochemistry (see Figure 24). The orders of nobility of the samples were again the same as their DoS, with the highest sensitized samples being the least noble. Orientation of the stress showed no contrast in results as samples with different stress orientation had a similar Tafel plot as other samples with the same DoS. Pitting potentials were not determined for the unsensitized samples, while sensitized samples had a distinguishable pitting potential that was more prominent as the sensitivity increased.

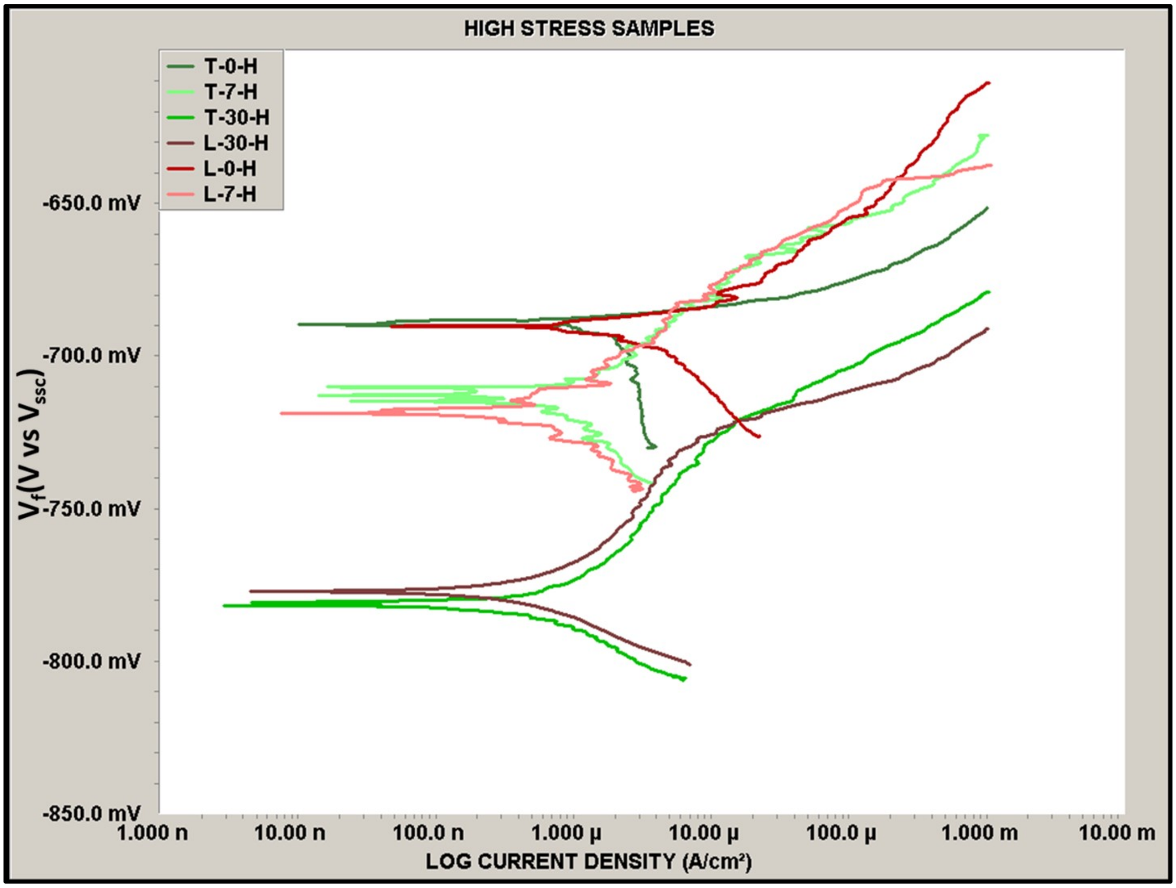

Figure 24. Potentiodynamic scans of samples under 200MPa applied tensile stress applied in different orientations with respect to the rolling direction.

F. POTENTIOSTATIC HOLDS

1. Open Circuit Potential Hold Images

Surface depth scans of the samples before the 72-hour OCP hold (see Figures 25 and 26) shows that there were no areas on the sample surfaces greater than -1 µm deep. Black specs indicate non reflective areas due to pullout from polishing. The polished surfaces were extremely reflective and a single light level was required to scan the surface areas. The intensity images before the OCP holds did show some surface scratches as well as minor pits/exclusions and pullout from polishing prior to exposure to saltwater (see Figure 25). The optical pictures and depth scans of the samples prior to the potentiostatic holds established a baseline for corrosion penetration.

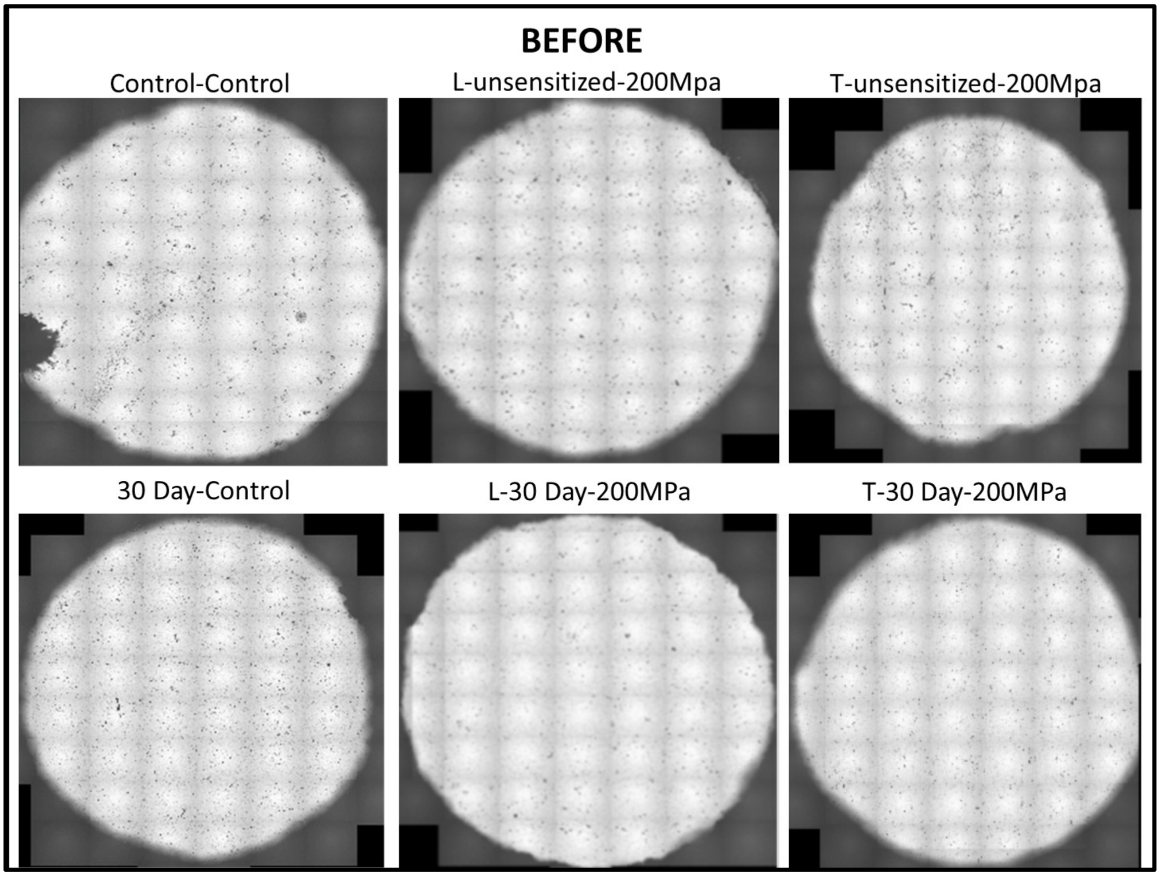

Figure 25. Stitched intensity images of samples before OCP hold (100x magnification, all surface areas are approximately .282 cm^2).

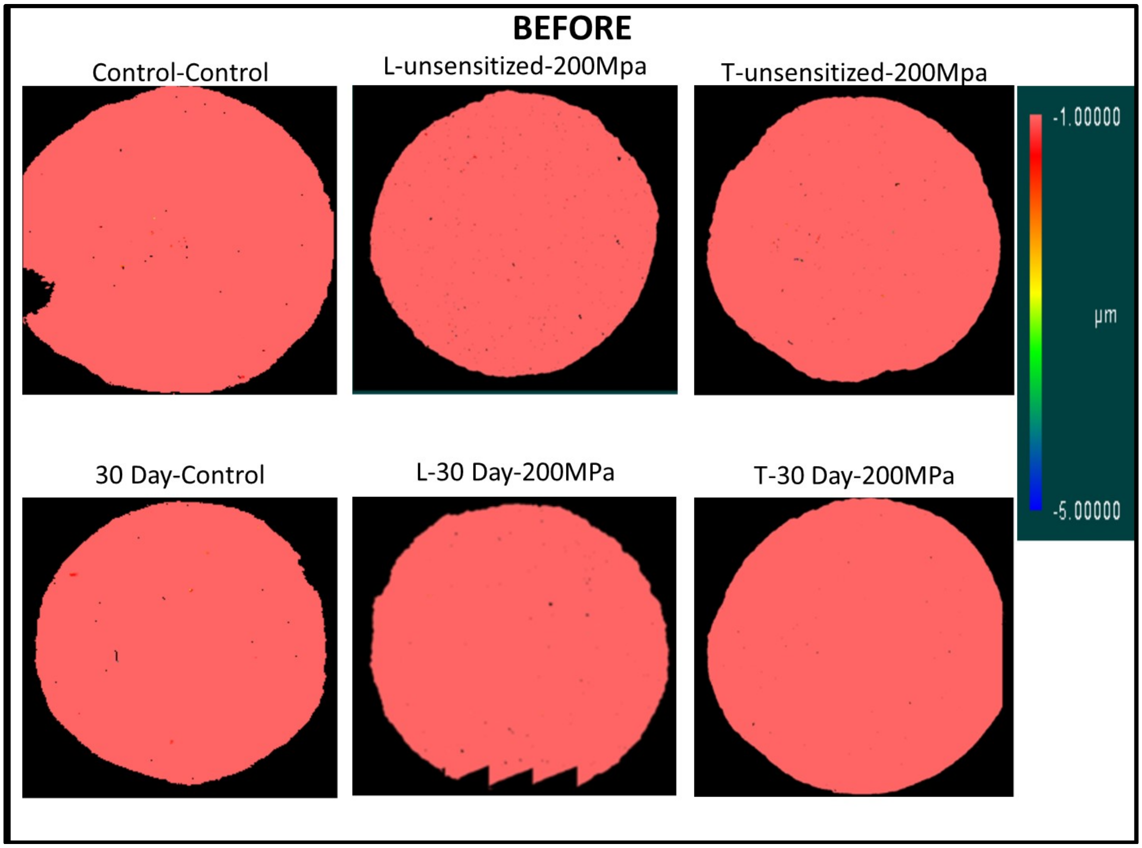

Figure 26. Stitched depth images of samples before OCP hold.

Samples after the 72-hour OCP hold displayed different types of corrosion and levels of damage based on their sensitization level, stress level, and stress orientation (see Figures 27–29, Table 6). The unsensitized, unstressed (Control-Control) sample displayed the least amount of damage and depth of penetration as expected, with the sample having minor pit formations with possible IGC forming from the biggest pits in the middle. The 30 Day sensitized control (unstressed) sample had similar surface damage to the Control-Control sample, but a greater fraction of surface area corrosion and depth of penetration. The stressed, unsensitized stressed samples had more generalized corrosion indicated by the large non-reflective areas shown as darker areas on the intensity images. The stressed, T-oriented, unsensitized sample had corrosion damage on the entire exposed surface, compared to the stressed, L-oriented, unsensitized stress sample that had both general corrosion and pitting corrosion. The stressed, sensitized samples displayed pit formations and IGC, with a larger area fraction of corrosion damage and depth of penetration compared to both of the control samples. The highly stressed, 30-day sensitized sample also had the most amounts of distinguishable pit formations but the depth of penetration was less than that of the stressed, unsensitized sample. Sensitized samples were prone to pitting corrosion while unsensitized samples had more generalized corrosion. Stressed unsensitized stressed samples had significantly deeper corrosion depths than the unstressed, unsensitized control sample. For the sensitized samples, the depth of penetration was comparable between the stressed and unstressed samples. Sensitized samples stressed in the T orientation had a deeper depth of penetration than sensitized samples stressed in the L orientation (see Figure 29, Table 6).

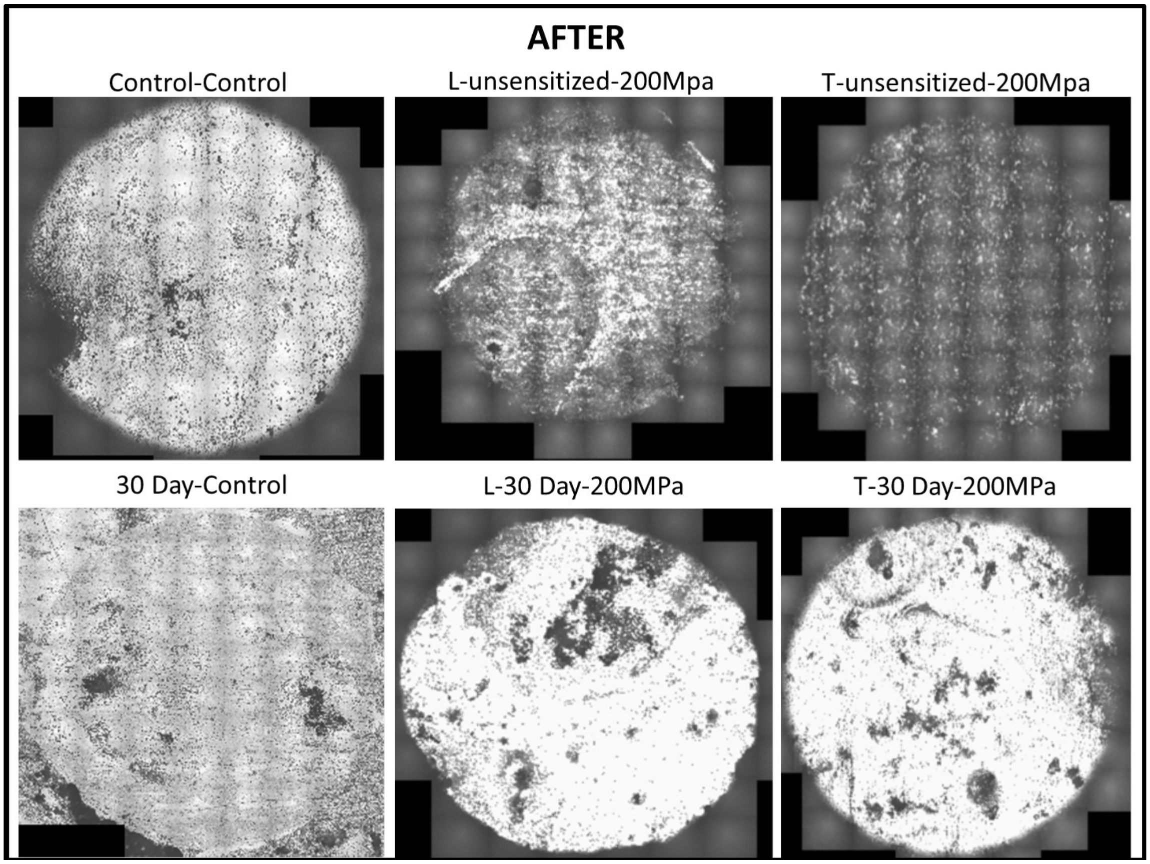

Figure 27. Stitched intensity images of samples after OCP hold (100x magnification, all surface areas are approximately .282 cm^2). Circles indicate exposed surface.

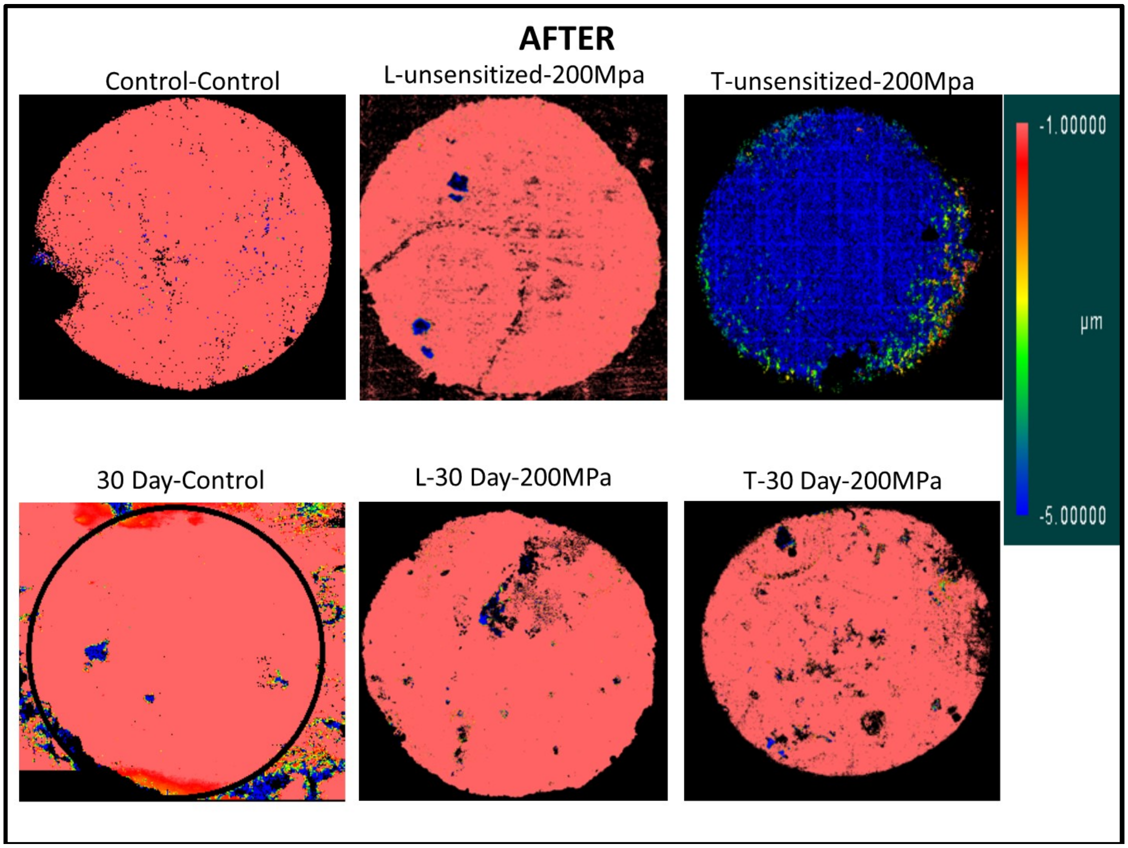

Figure 28. Stitched surface depth images of samples after OCP hold. Black overlay circle on the 30-day control sample indicates the exposed surface.

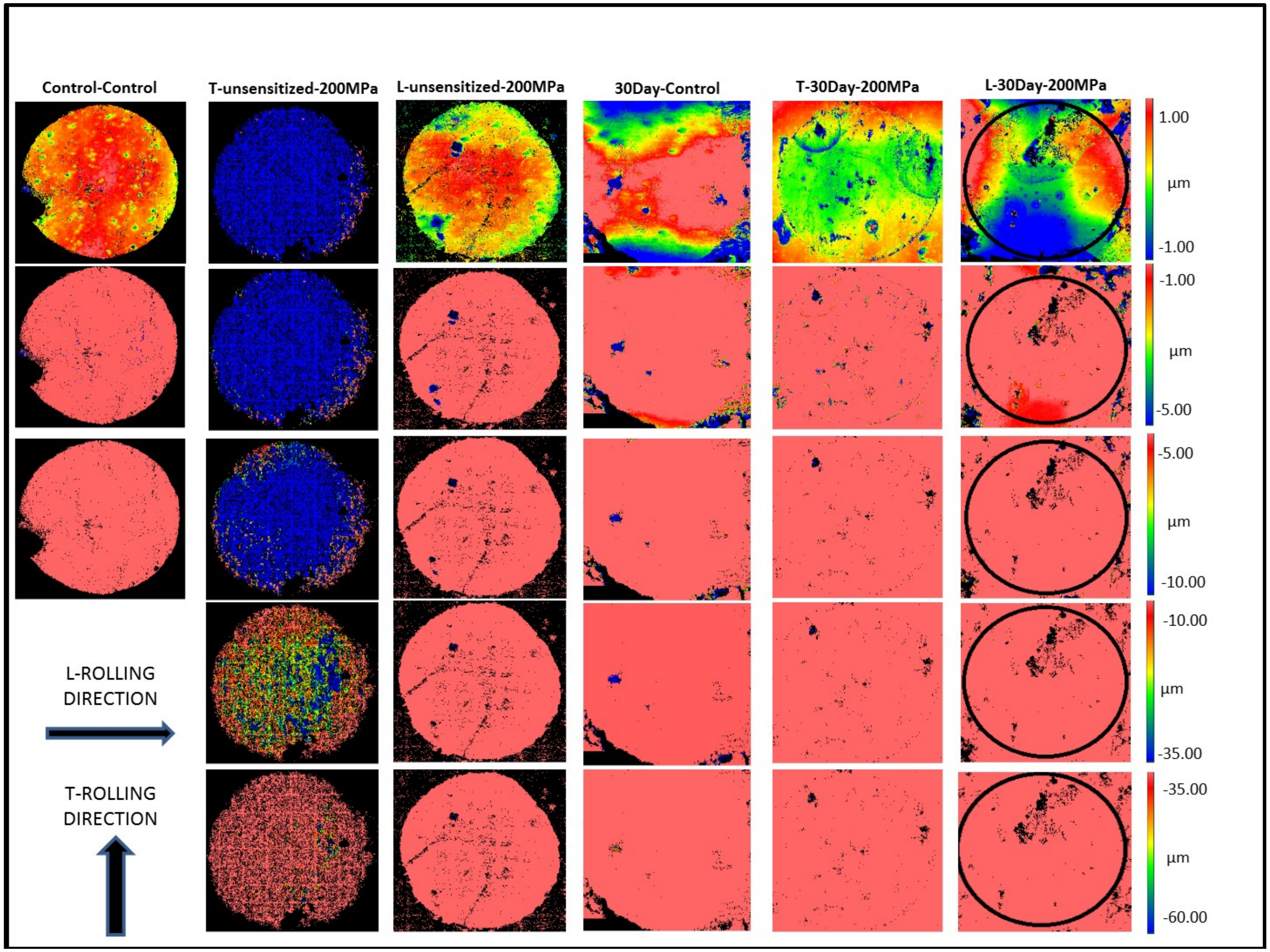

Figure 29. Corrosion depth comparison of samples after OCP hold using stitched surface depth image at various depth scales. Black circles are imposed to show exposed areas to saltwater.

2. Applied Potential Hold Images

As with the OCP hold images, the before applied potential hold samples show some surface scratches as well as minor pits/exclusions and pullout from polishing (see Figure 30). Surface depth scans of the samples before the applied potential hold (see Figure 31) showed there were no areas on the sample surfaces greater than -1 μm deep.

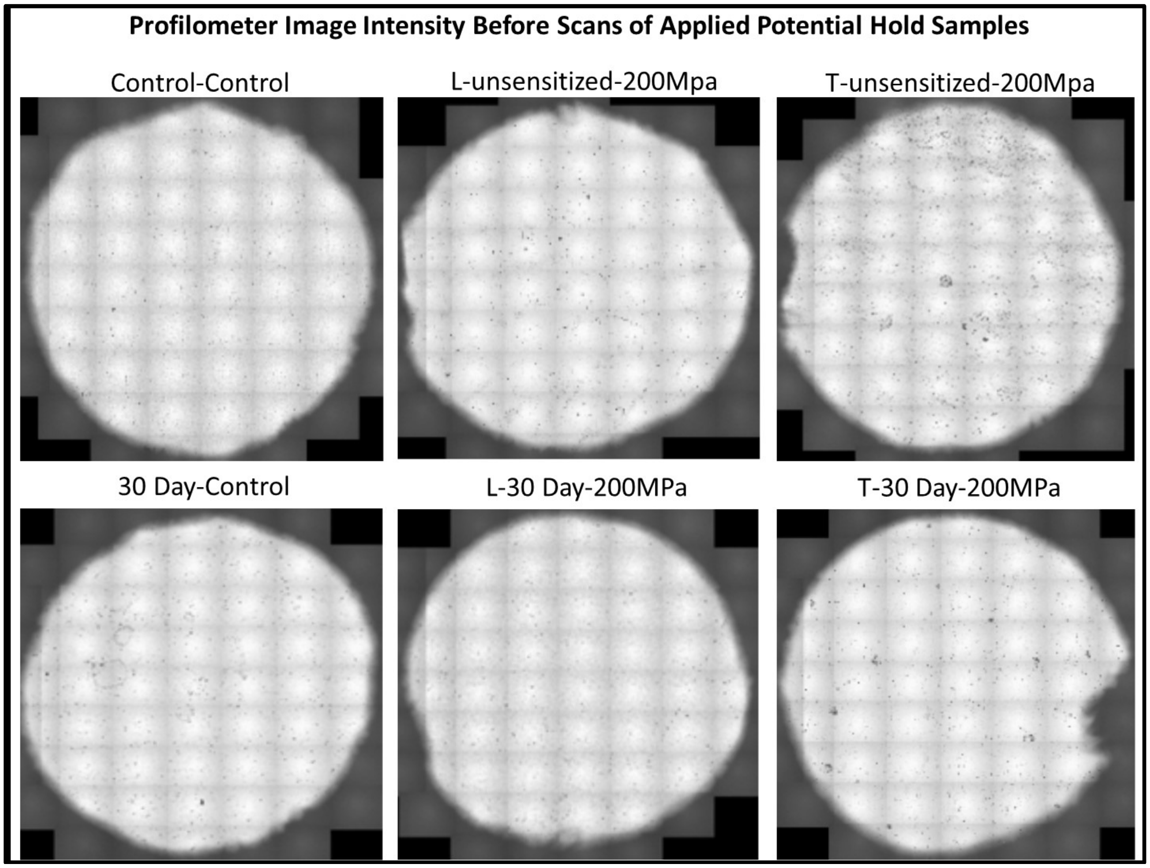

Figure 30. Stitched intensity images of samples before applied potential hold (100x magnification, all surface areas are approximately .282 cm^2).

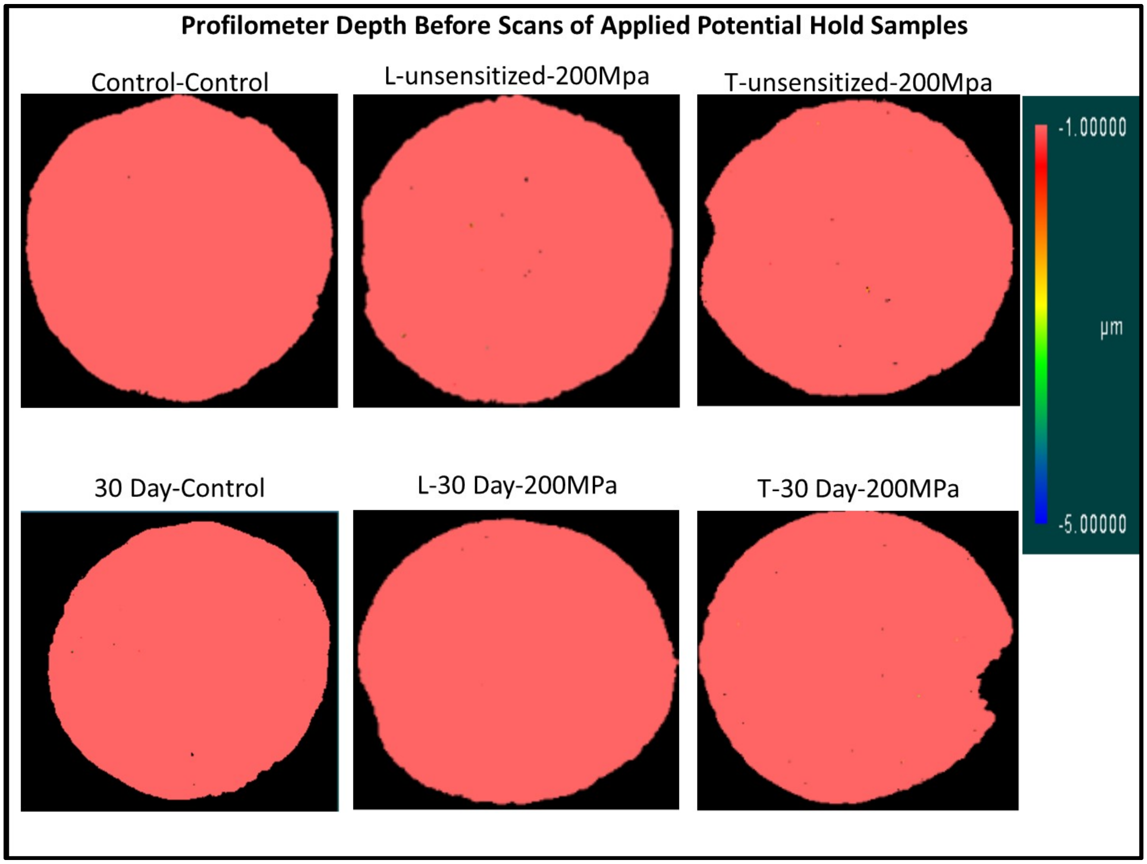

Figure 31. Stitched surface depth images of samples **before** applied potential hold.

Samples after the 72 hour applied potential (+35 mV over OCP) hold displayed different types of corrosion and levels of damage based on their sensitization level and stress orientation with some key differences from the same experiments at the OCP (see Figures 32–35, Table 7). As with the OCP hold experiments, the unstressed unsensitized (Control-Control) sample displayed the least amount of damage and depth penetration. The stressed, unsensitized stressed samples, for both orientations, again had generalized corrosion over the entire exposed area, just like with the OCP holds, but with more extensive corrosion damage. Unexpectedly, the unstressed, 30-day sensitized sample also had generalized corrosion on most of the exposed surface area. The stressed, sensitized samples displayed large and deep pit formations, which were the deepest corrosion penetrations of all of the experiments. As with the OCP hold experiments, the sensitized samples were prone to pitting corrosion (with the exception of the 30-day control sample) while unsensitized samples had more generalized corrosion. In addition, the stressed, T-orientation samples had the deeper corrosion penetrations compared to the stressed, L-orientation samples. In contrast with the OCP hold experiments, the stressed sensitized samples had significantly deeper corrosion depths than the unstressed sensitized control sample. Stressed samples also had significantly more corrosion damage than the unstressed samples. The effect of stress and the orientation that was applied was apparent in the applied potential experiments. The sensitization level played a key role in the type of corrosion that was present, but stress increased the magnitude of damage of the corrosion.

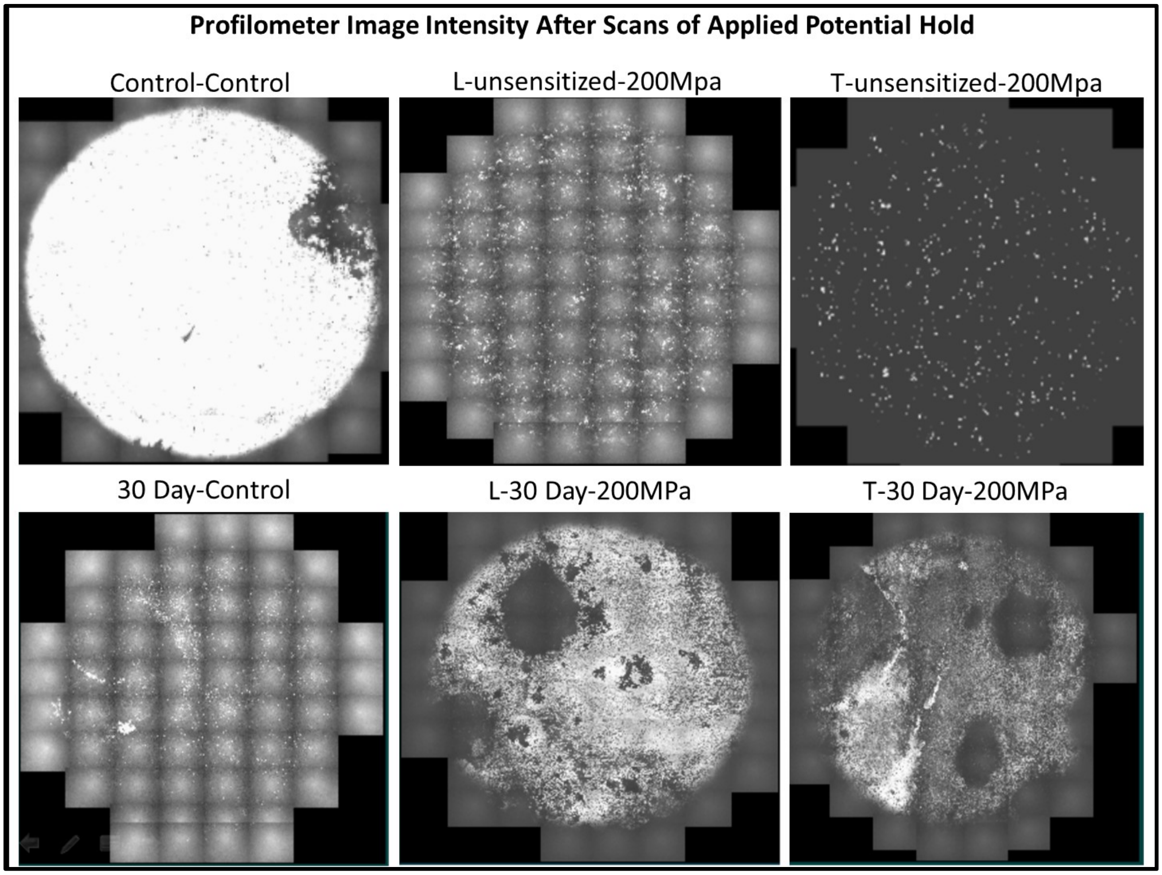

Figure 32. Stitched intensity images of samples after applied potential hold (100x magnification, all surface areas are approximately .282 cm^2).

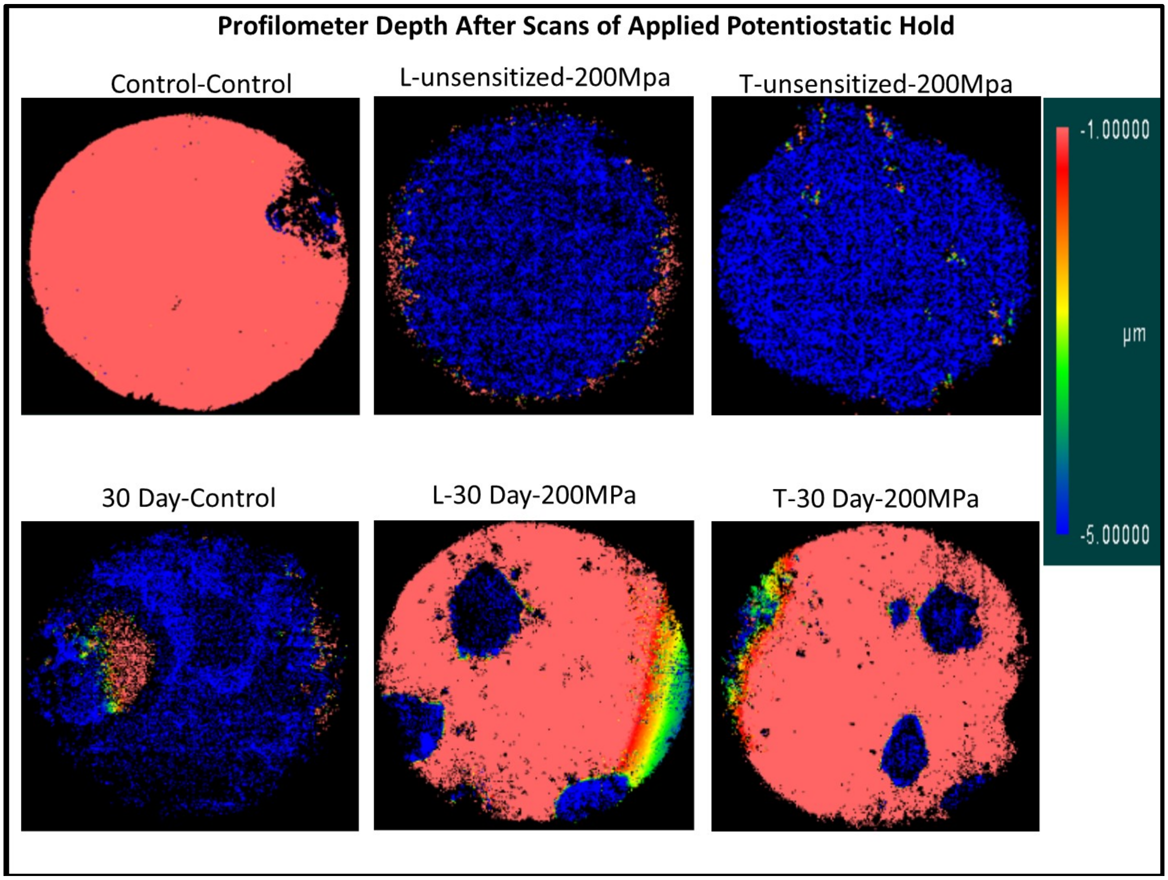

Figure 33. Stitched surface depth images of samples after the applied potential hold. Circles indicate area exposed to saltwater

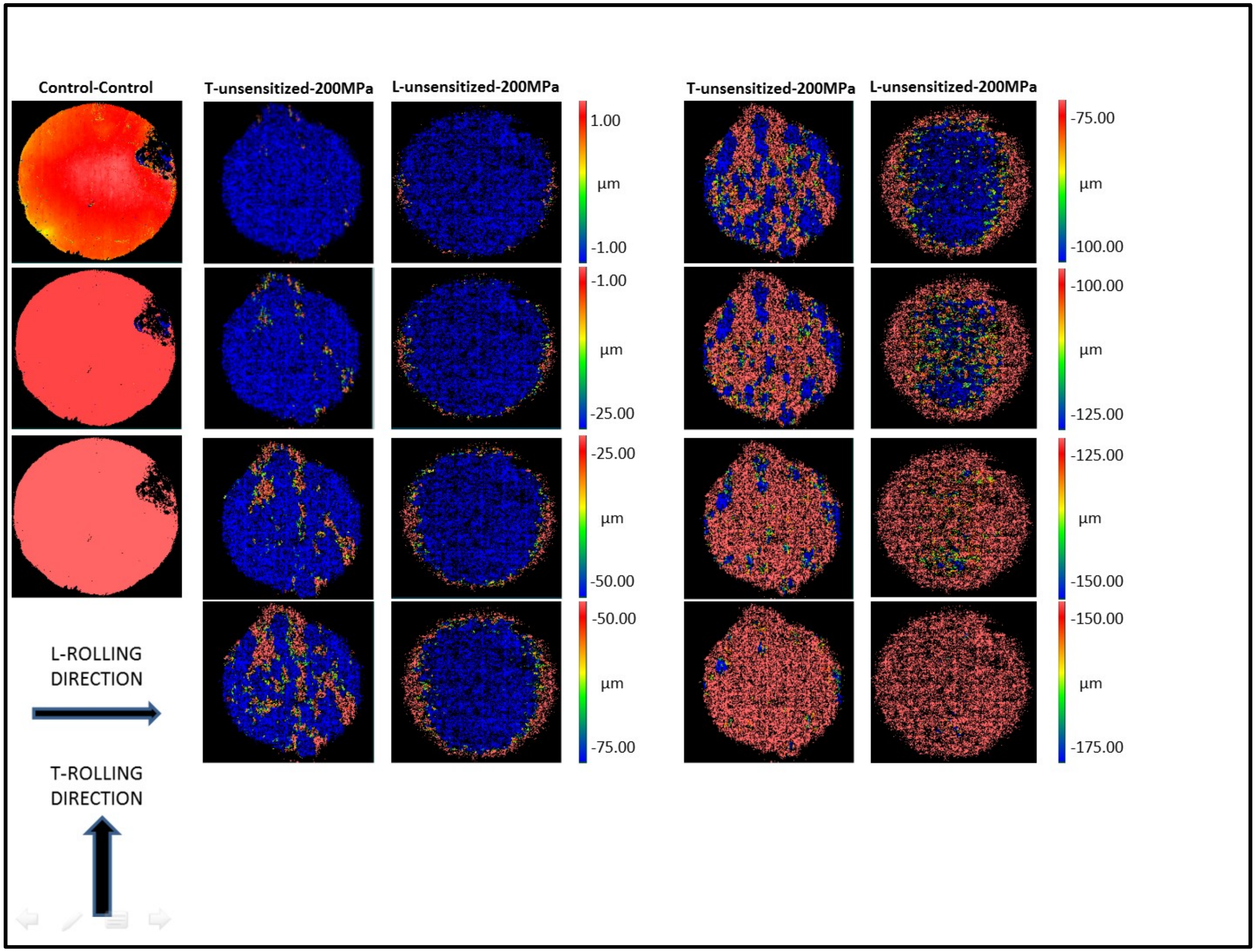

Figure 34. Corrosion depth comparison of unsensitized samples after applied potential holds using stitched surface depth image at various depth scales. The direction of applied stress is from left to right in these images.

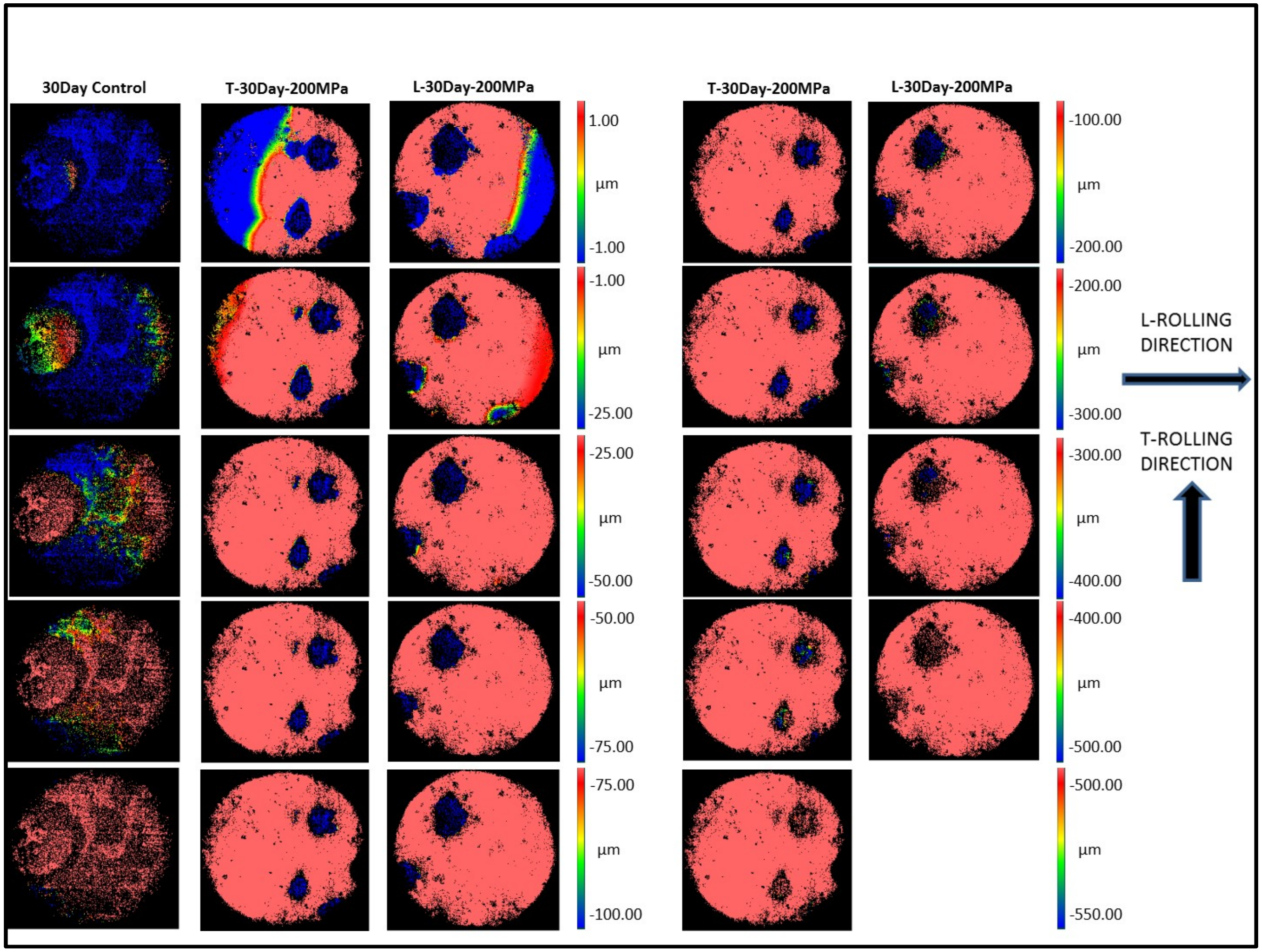

Figure 35. Corrosion depth comparison of sensitized samples after applied potential holds using stitched surface depth images at various depth scales. Right side of figure is the continuation of the stressed sensitized samples with different depth scales. The direction of applied stress is from left to right in these images.

Applied Potential Samples	Deepest Measured Corrosion Depth(µm)	Applied Potential (mV) (OCP+35mV)	PittingPotential (mV) (from potentiodynamic scan)
Control Control	-18	-652	not discernable
T-unsensitized 200MPa	-224	-654	not discernable
L-unsensitized 200MPa	-175	-655	not discernable
30 Day Control	-98	-765	-734.1
T-30 Day 200MPa	-513	-746	-728.6
L-30 Day 200MPa	-411	-742	-733.2

Table 7. Comparison of applied potential hold samples and their applied potential values, pitting potentials, and deepest measured corrosion penetration as measured by the optical profilometer.

THIS PAGE INTENTIONALLY LEFT BLANK

III. DISCUSSION

A. ROLE OF STRESS ON CORROSION

The effect of stress on localized corrosion of AA5083 was evident in the potentiodynamic and potentiostatic experiments, causing stressed samples to have more corrosion damage than unstressed samples. Comparison of unsensitized samples during the potentiostatic tests (see Figure 23) showed that stressed samples had a higher current density for a given potential (Table 5), leading to the possibility that stressed samples could have more extensive damage than unstressed samples exposed to saltwater. This result was evident in the potentiostatic experiments for both the OCP and applied potential holds. At both of these potentials, the stressed samples, regardless of sensitivity, showed considerably more corrosion damage than their unstressed counterpart when comparing the depth of penetration (Table 6, 7; Figures 29,34, 35) and the amount of surface area damaged (see Figures 27, 28, 32, and 33). During the OCP holds, the unsensitized stressed samples had extensively more damage than the unsensitized unstressed (control-control) sample, while the stressed, sensitized samples had comparable depth damage to the 30 day unstressed sample (Table 6). The deepest measured corrosion depth however does not show the extent of corrosion on the exposed area, where the stressed, sensitized samples had qualitatively more surface coverage of pits and IGC than the 30 day control sample. The applied potential holds also showed the stressed samples to have extensively more damage than the unstressed samples. Quantitative and qualitative evidence suggests that applied stress causes a greater extent of corrosion in a saltwater environment. This agrees with the work performed by Liu et al., who found that stress on AA2024 increased the penetration rate of intergranular corrosion when compared to unstressed samples [24].

he applied stress also caused systematic changes in the electrochemical potentials for corrosion, albeit in a somewhat surprising fashion. Stressed samples had a less negative OCP than unstressed samples, and the shift increased as the stress level increased (see Figures 24 and 25). The pitting potentials of the 30-day sensitized stressed and unstressed samples; however, remained comparable (see Figure 25). The smaller difference between the OCP and pitting potential caused a smaller passive range for the stressed samples than the unstressed samples (Table 5). It may be that it is the reduction in passive range, which drives more aggressive corrosion with an applied elastic stress, despite the upward (more noble) shift of the OCP itself. The behavior of the unsensitized samples may be driven by different factors. These samples did not have a shift of OCP due to applied stress (see Figure 23), yet they incurred a significant amount of general corrosion damage compared to the unstressed sample..

The direction of the applied stress had a minimal effect on the polarization curves but a measurable effect on depth of penetration after corrosion. Both sensitized and unsensitized samples stressed in the transverse direction had the deeper corrosion depths, especially after the applied potential holds (Table 7). This suggests that the orientation of stress played a physical role in IGC or IGSCC compared to electrochemical effects. These observations are in line with work performed by Lim et al. on AA5083 [11] and Liu et al on AA2024 [23], in which both found a relationship in the orientation of applied stress or applied potential to the penetration rate of IGC. This orientation effect was attributed to the longer grain boundary paths in the longitudinal and transverse directions caused by the anisotropic microstructure of AA5083. The orientation of stress could lead physical effects such as crack tip propagation, or electrochemical and metallurgical factors such as beta phase continuity along grain boundaries [24]. The major electrochemical effect based on orientation of stress can be seen in Figure 23 and Table 5, where the current density of unsensitized samples differed based on stress orientation. However, like Liu’s work [23], there was no difference in the Tafel plots of sensitized stressed samples (see Figure 24).

B. ROLE OF SENSITIZATION ON CORROSION

The largest difference between sensitized and unsensitized samples was the type of corrosion each had incurred, especially while stressed. Sensitized stressed samples had more localized pitting corrosion, while unsensitized stressed samples had more general corrosion, or possibly exfoliation corrosion over the entire exposed surface. Exfoliation corrosion usually requires sensitization to occur, yet the unsensitized sample displayed an intergranular attack leading to the possibility of exfoliation.

As expected, the DoS had the largest effect on electrochemistry during the potentiodynamic runs. The higher the DoS, the more negative the OCP of the sample (see Figure 26). This is comparable to Jain et al. work that showed that the difference in potentials between the aluminum matrix and the β phase was about 200 mV [11]. The more anodic β phase made the samples OCP shift based on DoS, with the highest sensitized samples being the most negative. The most sensitized samples also displayed a prominent pitting potential, leading to the conclusion that sensitized samples would be more likely to incur pitting corrosion than unsensitized samples. Jain's work also found that at potentials between the β phase pitting potential of -750mV$_{sce}$ (-705mV$_{Ag/AgCl}$) and the aluminum matrix pitting potential (average of-725mV$_{sce}$, or -680mV$_{Ag/AgCl}$) that IGC spreading is more likely to occur on the sample surface. The unsensitized unstressed sample OCP for this experiment was -687mV$_{Ag/AgCl}$ and the pitting potential for the 30 day sensitized samples was approximately -730mV$_{Ag/AgCl}$ (Table 6) are similar to the work of Jain et al. The slight differences may be the exact temperature of the alloy; Jain used AA5083-H131 and had somewhat different DoS values for their samples. However, the range where IGC spreading occurs still applies. This IGC spreading might explain the different types of corrosion damage seen between the sensitized and unsensitized stressed samples during the potentiostatic experiments in this thesis (see Figures 32 and 34). The unsensitized stressed samples displayed a more general corrosion, possibly an exfoliation form of corrosion over the entire exposed surface, while the sensitized stressed samples had localized pitting corrosion. During the OCP potentiostatic hold the unsensitized stressed samples were held at L -690V$_{Ag/AgCl}$ and T -689V$_{Ag/AgCl}$ while the stressed samples were held at L -777mV$_{Ag/AgCl}$ and T -781mV$_{Ag/AgCl}$. During the applied potential holds the unsensitized stressed samples were held at L -655V $_{Ag/AgCl}$ and T -654V$_{Ag/AgCl}$ while the stressed samples were held at L -742mV$_{Ag/AgCl}$ and T -746mV$_{Ag/AgCl}$. The unstressed samples' potentials could have fallen into the range of IGC spreading and exfoliation corrosion, where the sensitized samples were just below this range, possibly in the range of metastable pit formations at β phase sites on the surface [28]. The differences between potentials due to the differences in DoS could have led to the different types of corrosion observed between the sensitized and unsensitized samples.

C. EFFECTIVENESS OF CONFOCAL MICROSCOPY TO ASSESS CORROSION DAMAGE

Confocal microscopy was instrumental in qualitatively analyzing the exposed surfaces of the samples, as well as quantifying the depth of corrosion. The stitch function allowed for analysis of the entire exposed surface, producing easily comparable optical and color coded depth images. These depth images were easily scaled to show the penetrations on multiple levels of the surface. Yet, there were limitations on the experimentation using the current equipment. First, presence of IGC was not possible at the low magnification used (100x), and the use of other analyzing tools such as electron microscopy, SEM, or TEM would have been necessary to fully understand the scope of the corrosion at the microscale. A second higher magnification using the confocal microscope would have been useful to obtain higher resolution data. Second, the roughness and irregularity of pit shape makes accurate depth measurement of pits difficult. The confocal technique can only reliably determine the height of reflective surfaces. Higher x-y spatial resolution might help with this problem as well. Finally, more robust algorithms are needed to help automate the scanning process, as the learning curve was high to determine proper settings on the corrosion samples due to different surface reflectivity, and different required scanning lengths to measure the surface depths. Algorithms to combine light intensity scaling and multiple light intensities for a single area, and filter pertinent data would help reduce the number of black areas on the graphs, produce better quality images, and reduce the manpower to run the equipment.

IV. CONCLUSION

This thesis investigated the effects of applied stress on the localized corrosion of AA5083-H116 in 0.6M saltwater. In addition, this research considered the coupled variables of sensitization level and microstructural orientation in combination with the applied stress. These effects were analyzed using electrochemical potentiodynamic scans on samples at various applied stresses at various orientations with regards to the rolling direction of the alloy, and sensitization levels of the material. Before and after optical profilometer depth-profiles of samples held at fixed potentials for 72 hours were compared for samples with the same orientation, sensitization, and stress variables. This thesis showed that DoS, stress level, and stress orientation affected the localized corrosion of AA5083 in a saltwater environment.

1. Assess the effects of applied elastic stress on the localized corrosion of AA5083-H116 during electrochemical potentiodynamic and potentiostatic testing.

Applying an elastic tensile stress caused substantially more corrosion damage compared to an unstressed sample, which was particularly noticeable in the applied potential samples. Stress also caused a shift in the OCP of sensitized samples, but not in unsensitized samples.

2. Assess the effects of microstructural orientation with regard to applied tensile stress, and sensitization on the localized corrosion of AA5083-H116.

Samples stressed in the transverse direction had slightly deeper corrosion penetration compared to samples stressed in the longitudinal direction and unstressed samples. The differences in polarization curves and in type of corrosion were minimal between the two orientations. As expected, the electrochemistry of the samples was most influenced by the DoS, and the types of corrosion observed were different when comparing unsensitized and sensitized samples.

3. Implement optical profilometry to quantify localized corrosion.

By using optical profilometry, depth of corrosion was able to be measured, and whole sample surfaces were easily compared to determine the type and extent of corrosion. The current spatial resolution of the technique was insufficient for careful examination of intergranular corrosion. More powerful objective lenses and improved analysis algorithms will make optical profilometry a very powerful analytic tool for corrosion experiments.

LIST OF REFERENCES

[1] J. R. Scully et al., "Development and validation of an integrated intergranular corrosion/cracking model of Al-Mg alloys for naval applications," in *Workshop on Sensitization of Aluminum Alloy 5XXX Series*, 2011.

[2] R. Schwarting et al., "Manufacturing techniques and process challenged with CG47 class ship aluminum superstructures modernization and repairs," in *Fleet Maintenance & Modernization Symposium 2001: Assessing Current & Future Maintenance Strategies*, San Diego, CA, 2011.

[3] J. Searles et al., "Stress Corrosion Cracking of Sensitized AA5083 Al-4.5Mg-1.0Mn)," *Metallurgy and Materials Transactions A*, vol. 32A, 2859–2867, 2001.

[4] M. G. Fontana, *Corrosion Engineering*, New York: McGraw-Hill, 1987, pp. 820–824.

[5] D. A. Jones, *The Principles and Prevention of Corrosion*, 2nd ed., Upper Saddle River, NJ, Prentice Hall, 1996.

[6] M. N. James et al., "Residual stress and strain in MIG butt welds in 5083-H321 aluminum: As-welded and fatigue cycled," *International Journal of Fatigue*, vol. 31, no. 1, pp. 28–40, 2009.

[7] X. Liu et al., "Transition from intergranular corrosion to intergranular stress corrosion cracking in AA2024-T3," *Journal of the Electrochemical Society*, vol. 153, pp. B42–B51, 2006.

[8] B. Scott, "The role of stress in the corrosion cracking of aluminum alloys," M.S. thesis, Dept. Mech. and Aero. Eng., Naval Postgraduate School, Monterey, CA, 2013.

[9] The Aluminum Association, *International Alloy Designations and Chemical Composition Limits for Wrought Aluminum and Wrought Aluminum Alloys,* Arlington, VA: The Aluminum Association, 2009.

[10] M. A. Steiner et al., "Modelling sensitization of Mg-Al alloys via β-phase precipitation kinetics," *Scripta Materialia, v*ol. 102, pp. 55–58, 2015.

[11] M. L. Lim et al., "Intergranular corrosion penetration in an Al-Mg alloy as a function of electrochemical and metallurgical conditions," *Corrosion*, vol. 69, no. 1, 35–47, 2013.

[12] S. Jain et al., "Spreading of intergranular corrosion on the surface of sensitized Al-4.4Mg alloys: A general finding," *Corrosion Science*, vol. 59, no. C, pp. 136–147, Jun. 2012.

[13] ASM International, "Standard test method for determining the susceptibility to intergranular corrosion of 5XXX series aluminum alloys by mass loss after exposure to nitric acid," vol. G67-04, 2004, pp. 1–3.

[14] N. Dolić et al., "Pit nucleation on as-cast aluminum alloy AA-5083 in 0.01M NaCl," *Journal of Mining an Metallurgy,* vol. 47, pp. 79–87, 2010.

[15] M. M. Sharma, C. W. Ziemian, "Pitting and stress corrosion cracking susceptibility of nanostructured Al-Mg alloys in natural and artificial environments," *Journal of Materials Engineering and Performance*, vol. 17, pp. 870–878, 2008.

[16] N. Birbilis and R. Buchheit, "Electrochemical characteristics of intermetallic phases in aluminum alloys— An experimental survey and discussion," *Journal of Electrochemistry Society*, vol. 152, pp. B140–B151, 2005.

[17] M. K. Cavanaugh et al., "Modeling the environmental dependence of pit growth using neural network approaches ," *Corrosion Science,* vol. *52,* no. 9, pp. 3070-3077, 2010.

[18] R. K. Gupta et al., "Metastable pitting characteristics of aluminum alloys measured using current transients during potentiostatic polarization," *Electrochimica Acta* 66: 245–254, 2012.

[19] J. R. Brosi and J.J. Lewandowski, "Delamination of a sensitized commercial Al-Mg alloy during fatigue crack growth," *Scripta Materialia,* pp.799–802, 2010.

[20] Z. Foroulis and H. Uhlig, "Effect of Cold-Work on Corrosion of Iron and Steel in Hydrochloric Acid," *Journal of Electrochemistry Society*, vol. 111, no. 5, pp. 522–528, 1964.

[21] A. R. Despic, "Mechanism of the Acceleration of the Electrodic Dissolution of Metals during Yielding under Stress," *J Chem Phys*, vol. 49, no. 2, p. 926, 1968.

[22] N. Greene and G. Saltzman, "Effect of Plastic Deformation on Corrosion of Iron + Steel," *Corrosion*, vol. 20, no. 9, 1964.

[23] X. Liu et al., Effect of applied tensile stress on intergranular corrosion of AA2024-T3, *Corrosion Science*, vol. 46, no. 2, February 2004, pp. 405–425.

[24] X. Liu et al., "In-situ observation of intergranular stress corrosion cracking in AA2024-T3 under constant load conditions," *Corrosion Science*, vol. 49, pp. 139–148, 2007.

[25] J. Sanders, "The effects of applied stress and sensitization on the passive film stability of AL-MG alloys," M.S. thesis, Dept. Mech. and Aero. Eng., Naval Postgraduate School, Monterey, CA, 2013.

[26] ASM International, “Standard specification for high magnesium aluminum-alloy sheet and plate for marine service and similar environments,” vol. B928/B928M, 2009.

[27] ASM International, “Standard practice for preparation and use of bent-beam stress-corrosion test specimens,” vol. G39-99, *ASTM International*, pp.1–8, 2011

[28] R. K. Gupta et al., “Electrochemical Behavior and Localized Corrosion Associated with Mg_2Si Particles in Al and Mg Alloys,” *ECS Electrochemistry Letters* 1(1): B1–B3, 2012.

THIS PAGE INTENTIONALLY LEFT BLANK

INITIAL DISTRIBUTION LIST

1. Defense Technical Information Center
   Ft. Belvoir, Virginia

2. Dudley Knox Library
   Naval Postgraduate School
   Monterey, California